Performance of a perovskite-structured calcium manganite oxygen carrier produced from natural ores in a batch reactor and in operation of a

Chemical Engineering Journal 497 (2024) 154516

Contents lists available at ScienceDirect

Chemical Engineering Journal

journal homepage: www.elsevier.com/locate/cej

Performance of a perovskite-structured calcium manganite oxygen carrier produced from natural ores in a batch reactor and in operation of a chemical-looping combustion reactor system

Xiaoyun Li [a,*], Robin Faust [b], Victor Purnomo [b], Daofeng Mei [c], Carl Linderholm [a], Anders Lyngfelt [a], Tobias Mattisson [a]

[a] Department of Space, Earth and Environment, Chalmers University of Technology, 412 96 Gothenburg, Sweden
[b] Department of Chemistry and Chemical Engineering, Chalmers University of Technology, 412 58, Gothenburg, Sweden
[c] Instituto de Carboquímica, Consejo Superior de Investigaciones Científicas (ICB-CSIC), 50018 Zaragoza, Spain

ARTICLE INFO

Keywords:
Chemical looping with oxygen uncoupling
Oxygen carrier
Calcium manganite
Perovskite structure
Simple production method
Manganese ore

ABSTRACT

The potential for low cost of CO_2 capture using chemical-looping combustion (CLC) should not be compromised by costs associated with the oxygen carrier. This justifies studies of oxygen carrier materials with reasonable production costs. In this study, a perovskite calcium manganite ($CaMnO_{3-\delta}$), was synthesized from manganese ore and limestone through a straightforward process involving mixing with polyvinyl-alcohol, sintering, crushing and sieving. The calcium manganite produced exhibited two primary crystalline phases: $CaMnO_3$ (perovskite) and $CaMn_2O_4$ (marokite). Experiments were conducted using both a batch fluidized-bed reactor and a 300 W CLC reactor system in continuous operation to assess the oxygen uncoupling and reactivity of the calcium manganite. The results show that the oxygen uncoupling ability increases with temperature. Full syngas conversion was achieved at relatively low temperatures and low fuel-reactor bed mass over fuel power ratio in the 300 W unit. Elevated temperatures and ratio of fuel-reactor bed mass over fuel power enhance methane conversion significantly. The attrition of the calcium manganite was low, around 0.1 wt%/h for the last 15 h operation with methane. Batch reactor tests of fresh and used materials showed that there was no reduction in reactivity after 29 h of fuel operation.

1. Introduction

Chemical-looping combustion (CLC) of renewable biomass with carbon transportation and storage as shown in Fig. 1 is a promising technology for atmospheric CO_2 removal that can provide power/heat with higher efficiency. CLC can also be used with other fuels as well as in combination with steam methane reforming to produce blue hydrogen [1]. In contrast to conventional combustion, CLC employs two interconnected fluidized-bed reactors: the air reactor (AR) and the fuel reactor (FR). In the AR, oxygen carrier particles, typically metal oxides, are oxidized by oxygen in air. Subsequently, these oxidized oxygen carriers are transported to the FR, where they are reduced by the fuel. The resulting reduced oxygen carriers then circulate back to the AR to be regenerated for a new redox loop. One of the key advantages of CLC is its inherent CO_2 capture without the need for costly and energy-intensive gas separation processes. Additionally, as the AR is devoid of fuel, the absence of fuel contaminants in the AR flue gas allows for higher-temperature heat extraction, i.e. raised steam data. Conversely, fuel contaminants, such as SO_x, NO_x and aggressive ash contaminants like alkali, are concentrated in the flue gas of FR [2].

CLC has been successfully implemented in more than 49 pilot-scale units, ranging from 0.2 kW to 3 MW for more than 11,000 operational hours with gaseous, liquid, and solid fuels. This establishes CLC as a well-proven technology in small pilot-scale units [3]. However, additional challenges may arise during the upscaling process. As the technology moves from pilot-scale to larger operational scales, factors such as increased system complexity, optimal fluidization, fuel conversion in FR and the development of robust and economically feasible oxygen carriers become even more critical. Two important costs of the CLC process stem from oxygen production for conversion of remaining combustible gases in the exit of FR and oxygen carrier expenses. The latter is closely related to the fuel conversion in FR and thus the need for

* Corresponding author.
E-mail address: xiaoyun.li@chalmers.se (X. Li).

https://doi.org/10.1016/j.cej.2024.154516

Available online 3 August 2024

oxygen [4,5]. Hence, to assure the economic viability of CLC on a large scale, it is imperative to identify cost-effective oxygen carriers preferably characterized by high reactivity and long lifetimes.

Once the solid fuel is introduced into the hot FR, it undergoes devolatilization, resulting in the formation of volatiles and char. The char subsequently undergoes a slow gasification process. In regular CLC, volatiles and gases from char gasification react with the oxidized oxygen carriers coming from the AR. However, in chemical looping with oxygen uncoupling (CLOU), the conversion of volatiles and char in FR can be notably enhanced [6–13]. This is attributed to the ability of oxygen carriers in CLOU to release oxygen to the gas phase. The process distinction of regular CLC and CLOU is illustrated in Fig. 2.

In CLOU, the oxidized oxygen carrier coming from the AR releases gaseous oxygen, and then the volatiles and the char directly react with oxygen in gas phase, thus avoiding the slow char gasification step and improving the conversion of volatiles. Consequently, CLOU oxygen carriers should have the ability to both release and capture oxygen under appropriate temperatures and oxygen partial pressures. Three such potential metal oxide systems with suitable thermodynamic properties for CLOU have been investigated, namely CuO/Cu_2O, Co_3O_4/CoO, and Mn_2O_3/Mn_3O_4 [6,14–18]. Copper has been extensively investigated and has high performance for CLOU. However, copper oxide materials have poor physical integrity and a melting point of 1085 °C, which could give short lifetime and high risk of agglomeration and defluidization [12,15,17]. The health, safety and environmental issues make cobalt oxides system as CLOU oxygen carriers unattractive [12]. Furthermore, both copper and cobalt are costly metal resources whereas manganese is quite abundant. A low temperature is required for the reoxidation to Mn_2O_3 in AR, which also means a slow reaction rate in the AR [12]. However, manganese ions can exist in remarkably multiple oxidation states from Mn^{2+} to Mn^{7+}. It is possible to alter its properties, i.e. mechanical strength and reactivity towards different fuels, by combining it with other elements, such as the binary systems $(Mn_yFe_{1-y})O_x$, $(Mn_ySi_{1-y})O_x$, $(Mn_yNi_{1-y})O_x$, $(Mn_yMg_{1-y})O_x$, $(Mn_yCu_{1-y})O_x$ [7–10,12,15,19,20], and ternary systems such as Mn-Fe-Si, Mn-Fe-Mg, Mn-Fe-Ti [21,22]. More importantly, the combinations change the thermodynamics, thus influencing the CLOU properties. For the combined manganese oxides, the O_2 uncoupling is associated with more complex phases changes, such as from bixbyite $(Mn_xFe_{1-x})_2O_3$ to spinel $(Mn_xFe_{1-x})_3O_4$, or from braunite Mn_7SiO_{12} to rhodonite $MnSiO_3$.

In addition to the above systems, the Mn-Ca system can form calcium manganite ($CaMnO_{3-\delta}$), which has a stable perovskite structure being able to release O_2 without changes of the phase structure. A common practice is to replace a small fraction of manganese with another element. Iron (Fe), titanium (Ti), and magnesium (Mg) are suggested as promising substitutions for part of manganese in calcium manganite [23–28]. $CaMn_{0.9}Mg_{0.1}O_{3-\delta}$ has been tested in a CLC pilot of 10 kW_{th}, demonstrating superior fuel conversion and minimal attrition when compared to benchmark ilmenite and Ni-based oxygen carriers [29,30]. It was also found that the Mg cation stays in MgO phase and is not incorporated into the perovskite structure and the active compound is likely pure $CaMnO_{3-\delta}$ [24,31]. But the addition of magnesium can improve fuel conversion, mechanical stability and fluidization properties [31]. Fe atoms can go into the perovskite structure replacing the Mn atom and improving the oxygen uncoupling and reactivity to methane [23,31,32]. Also, Ti could be used to replace a small amount of Mn to restrict the decomposition of $CaMnO_3$ to Ca_2MnO_4 and $CaMn_2O_4$ at high temperature, which might affect the full reoxidation of $CaMnO_3$ in AR [33,34]. Almost full conversion of natural gas could be achieved by $CaMn_{0.875}Ti_{0.125}O_3$ in a 300 W CLC reactor system with the physical properties being retained [11]. Industrial-scale production of the perovskite oxygen carrier $CaMn_{0.5}Ti_{0.375}Fe_{0.125}O_3$ from commercial raw material powders made with spray drying, showed similar chemical and physical properties as particles from small-scale production [35]. A comprehensive review of pressurized chemical looping processes by Osman et al. [36] suggests maximizing the energy efficiency of CLC. However, it was found that higher pressure negatively affects CO conversion when using calcium manganite-based oxygen carriers due to the inhibited O_2 release ability at relatively higher pressures [37].

Nevertheless, to investigate the potential for using low-cost raw

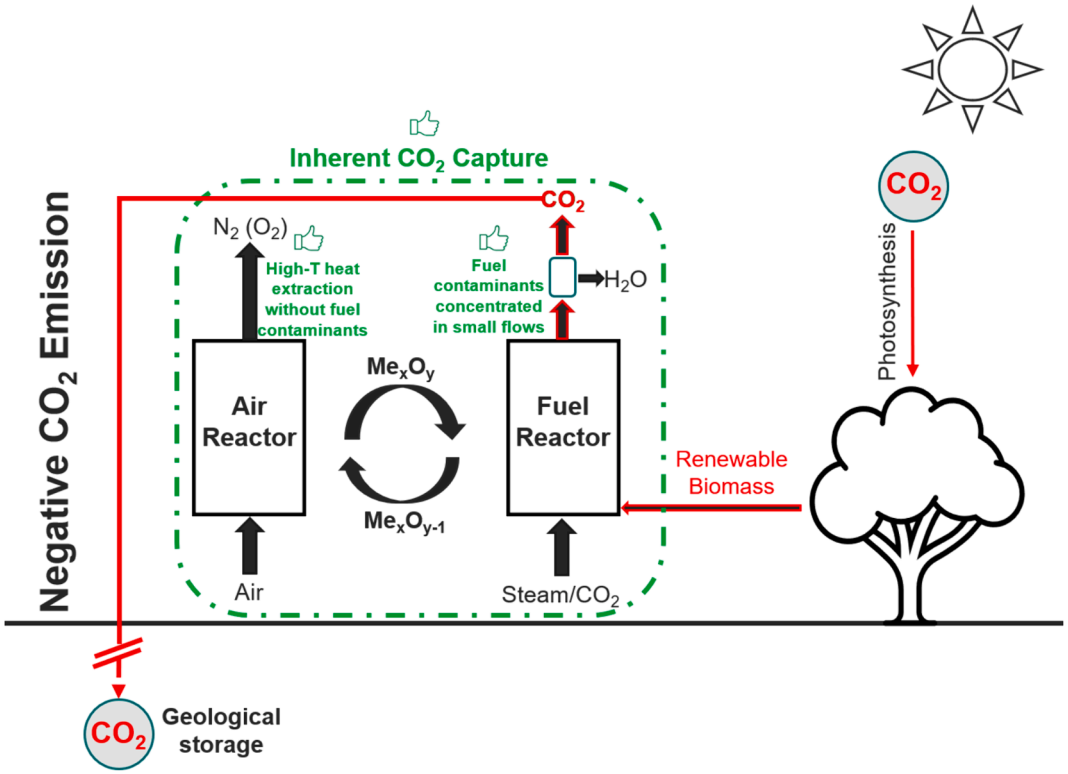

Fig. 1. Chemical-looping combustion of renewable biomass as a carbon removal technology.

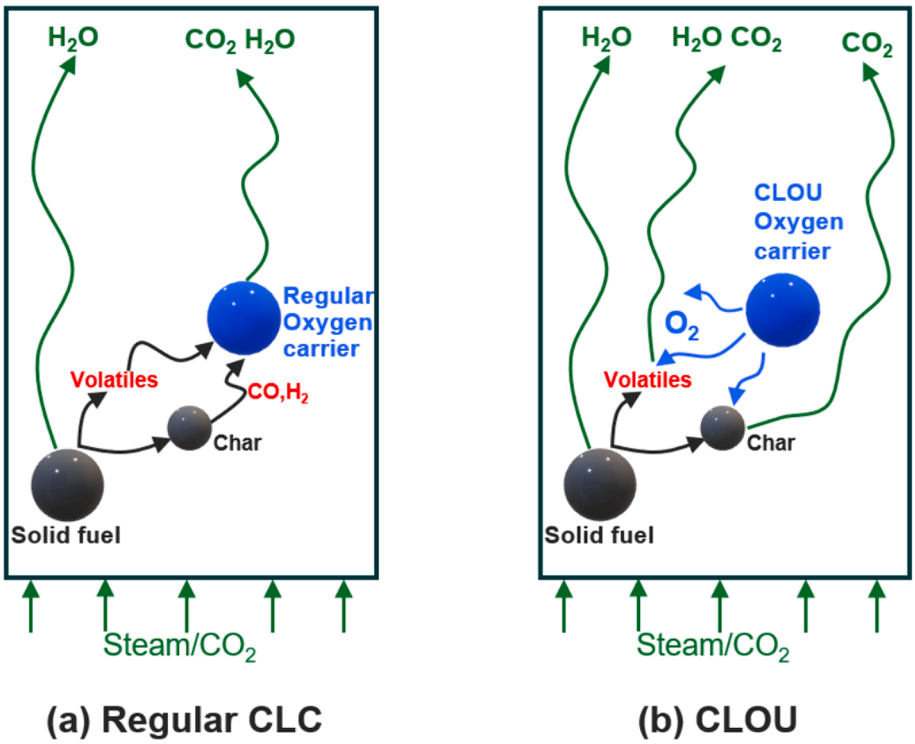

Fig. 2. Illustration of solid fuel conversion in fuel reactor for regular CLC and CLOU.

materials, this study explores the feasibility of making perovskite-structured calcium manganite from commercial and abundant natural ore particles of larger sizes and manufactured using simplified technologies suitable for large-scale production. The presence of impurities in the natural ores is not necessarily a problem but could potentially improve the stability and reactivity of the resulting calcium manganite product, as some of the impurities, especially Fe, could stabilize the perovskite structure, as has been previously shown [23,31,32].

2. Materials and methods

2.1. Production of calcium manganite particles

The oxygen-carrier particles used in this study were manufactured from limestone and Eramet HM manganese ore. The Eramet HM manganese ore is supplied by Eramet and originates from Gabon. The calcium carbonate content in the limestone provided by Faxe Kalk A/S is more than 96 wt%. The elemental composition of Eramet HM manganese ore is given in Table 1.

The raw materials were ball-milled and sieved to obtain particles smaller than 90 μm. For each batch of resulting oxygen carriers, a blend was formed by mixing 69.00 g Eramet HM manganese ore particles and 55.35 g limestone particles smaller than 90 μm. Subsequently, 11.79 g of a 10 wt% polyvinyl-alcohol solution was continuously added to the blend for binding and granulation. The mixture was then sintered in a box furnace at 1240 °C for 9 h. Following sintering, the mixture was crushed and sieved into particles ranging from 90 to 250 μm. The resulting particles exhibited irregular shapes as shown in Fig. 3, with a bulk density of 1102 kg/m^3 and an average crushing strength of 2.87 N. It has been reported that particles with a crushing strength above 2 N are highly likely to exhibit favorable performance with respect to attrition [38]. These particles were used in the testing phase in both the batch fluidized-bed reactor and the 300 W CLC reactor system. Compared to the fresh calcium manganite particles, the used particles in the 300 W CLC reactor become more rounded and smaller, as shown in Fig. 3 and Table 6.

2.2. Experimental setup

2.2.1. 300 W CLC reactor system

The oxygen carrier was investigated in a 300 W CLC unit with interconnected fluidized beds, thus enabling continuous operation with gaseous fuels [2]. The study assessed the CLOU effect of the oxygen carriers, their reactivity towards syngas and CH_4, as well as the integrity of the particles. A schematic illustration of the 300 W CLC reactor and the gas sampling system used in this work are shown in Fig. 4.

The 300 W reactor is constructed from 253MA, a high-temperature chromium-nickel stainless steel alloy well-suited for severe conditions. The reactor system is 300 mm high and comprises a fuel reactor (FR) with a cross-section of 25 mm × 25 mm and an air reactor (AR) with a cross-section of 25 mm × 42 mm. The upper part of AR narrows to a cross-section of 25 mm × 25 mm, raising the gas velocity to facilitate upwards transport of particles and ensuring the circulation of the oxygen carrier. There is a gap between the two reactors to eliminate the risk of

Table 1
Elemental compositions of Eramet HM manganese ore [2].

Mn Ore	LOI* (wt%)	Elemental compositions (wt%)									Total elements§ (wt%)
		Mn	Fe	Al	Si	K	Ba	Ti	Ca	Mg	
Eramet HM	0.90	53.60	7.10	4.50	1.70	1.10	0.37	0.14	0.07	0.06	68.64

* LOI=Loss on ignition, i.e., weight reduction of the heat-treated sample upon heating to 1000 °C in air.
§ wt% missing to 100% is oxygen.

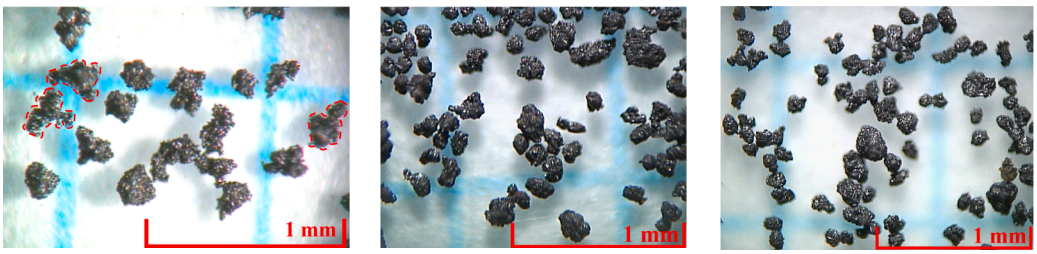

Fig. 3. Light microscope photos of calcium manganite particles: (a) fresh, (b) used particles after 2 h operation with syngas, (c) used particles after 29 h operation with CH_4.

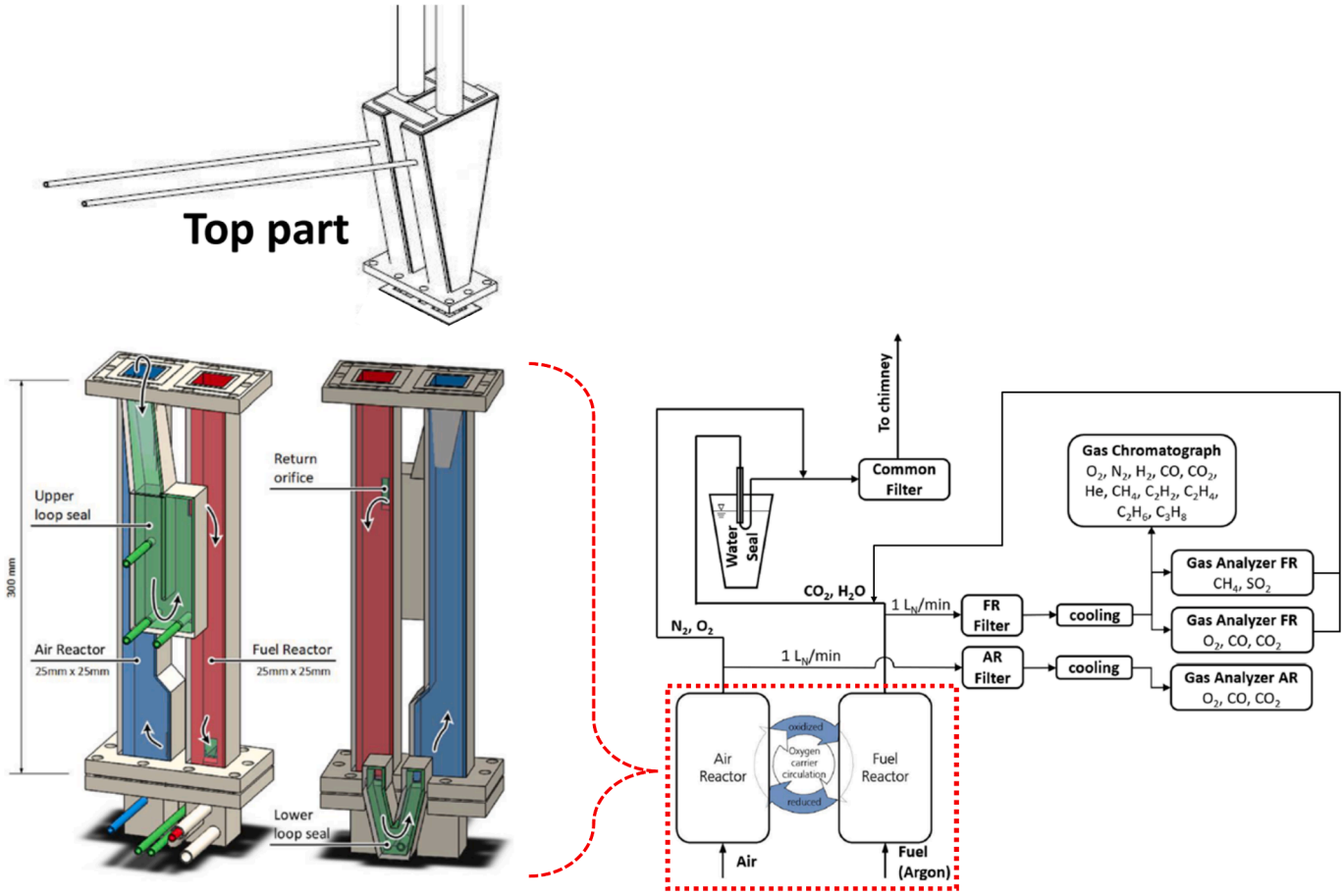

Fig. 4. 300 W reactor with the top part (left) and gas sampling system (right).

air leakage from AR to FR due to the improper welding.

The cross section of the top part above the reactors widens, shown in Fig. 4, to allow elutriated particles to fall down. A part of the particle flow falls into the upper loop seal and is transported into the FR through the return orifice. Particles located at the bottom of the FR pass through the lower loop seal and return to the AR, initiating a new cycle and completing the circulation of particles. The loop seals are purged with a flow of argon to ensure fluidization, circulation of particles, and that the gases in the AR and FR are kept separated. There are wind boxes located below the reactors leading the gas flow into the reactors via porous quartz plates which act as gas distributors.

The exit pipe of the FR is connected to a water seal with a column height of around 2 cm to maintain a 0.2 kPa higher pressure in the FR compared to AR in order to reduce the risk of gas leakage from AR to FR through the loop seals. The bed temperature of AR and FR is measured by means of K-type thermocouples. The 300 W reactor is subject to high heat losses due to a high surface-to-volume ratio. Hence, it is located inside a well-insulated electrical furnace that controls the temperature of the reactor, typically 800–950 °C. The fluidization and particle circulation are monitored via pressure difference measurements at different heights of AR and FR, as well as in the upper loop seal.

The investigations in the 300 W reactor system with calcium manganite, involved oxygen release ability (CLOU effect), reactivities towards syngas and methane, and attrition. The basic settings for each campaign are shown in Table 2. Syngas consists of 50 vol% of H_2 in CO with the lower heating value 11.7 MJ/m^3_n. The methane has a purity of 99.5 % and the lower heating value as 35.8 MJ/m^3_n.

The initial solids inventory of fresh calcium manganite sample is 300 g for both syngas and CH_4 campaigns. In addition to the gaseous fuel tests, the CLOU effect of the oxygen carrier particles is measured with argon flowing through FR. The test matrix for those campaigns is shown

Table 2
Operational conditions employed for different experimental campaigns.

Campaign	AR air flow (L_n/min)	FR gas	FR gas flow (L_n/min)	Fuel input (W)	FR temperature (°C)
CLOU	8	Argon	1	0	850–950
Syngas	8	CO&H_2	1	80–319	850–915
Methane	8, 9	CH_4	1	96–306	850–950

in Table 3. After 2 h syngas operation, 4.5 h CH_4 operation and 29 h CH_4 operation, the reactor system was cooled down in air atmosphere and oxygen carrier samples were taken from AR for characterization and batch-reactor tests.

2.2.2. Batch fluidized-bed reactor system

Both fresh and used calcium manganite samples were tested with respect to their oxygen uncoupling ability and reactivity towards methane and syngas at different temperatures in a batch fluidized-bed reactor system, which is illustrated in Fig. 5. The used calcium manganite sample was taken from the AR of 300 W unit after 29 h operation with CH_4.

The batch fluidized-bed reactor, suspended in an electrical furnace, is essentially an 820 mm-long quartz reactor with an inner diameter of 22 mm. Particles can be placed on a porous quartz plate located at 370 mm from the bottom. Gas is fed into the bed from the bottom through fine channels in the quartz plate. The pressure drop over the bed of particles is measured to monitor the fluidization status. A heating band is installed around the top of the reactor to prevent gas condensation. Two Type-K thermocouples measure the temperature inside the fluidized bed and below the quartz plate. The flows of oxidizing gases, i.e. 5 % O_2 in N_2, inert gases, i.e. pure N_2, and reducing gases, i.e. 100 % CH_4 or syngas, i.e. 50 % CO in H_2, are controlled using magnetic valves. After cooling down of the flue gas from the reactor with a cooler, the volumetric flow and gas concentrations of CH_4, CO, H_2, CO_2 and O_2 are measured using a Rosemount NGA 2000 multi-component dry gas analyzer. Nondispersive infrared sensor, paramagnetic oxygen sensor, and thermal conductivity sensor with a repeatability of less than 1 % are used to measure the concentrations of carbon-based gases, O_2 and H_2. Leion et al. [39] have presented a detailed presentation of the experimental system.

During the oxidation period, a flow rate of 900 mL_n/min of 5 vol% O_2 in N_2 was maintained, while 600 mL_n/min of N_2 and 450 mL_n/min of CH_4 or 900 mL_n/min of syngas were employed during the inert and reduction periods. These flow conditions induce a bubbling fluidization regime of the bed. The oxidation period continued until the O_2 concentration returned to 5 %, indicating the completion of particle oxidation. The experimental procedures in the batch fluidized-bed reactor system are summarized in Table 4.

Tests with silica sand served as blank experiments. 15 g samples were placed on the plate for O_2 uncoupling and CH_4 tests. It is not expected that sand would have any CLOU properties but is used in order to characterize the reactor system and establish the degree of back mixing of gases when switching between different conditions. Further, 2 g samples mixed with 13 g silica sands were used for syngas tests. The O_2 uncoupling tests aim to evaluate the oxygen release at different temperatures. For the tests with silica sand as blank experiments, the duration for oxidation and inert was set to 300 and 600 s, respectively. For the tests with both fresh and used calcium manganite samples, these periods were extended to 600 s and 1000 s. The reactivity of CH_4 and syngas towards different bed material samples was also evaluated in the batch reactor system. The gaseous fuels underwent cycles of oxidation, inert, reduction, and inert periods, with durations of 600 s, 90 s, 20 s, and 90 s, respectively. Four cycles of syngas tests were conducted for activation before CH_4 tests with the fresh calcium manganite sample. The purpose of this activation is to stabilize the reactivity and structure of the oxygen carriers. Experience shows that the reactivity in the first cycles often deviates from the following cycles. Once the fuel conversion appears stable across different redox cycles during activation, the oxygen carriers are considered to be well activated. The details about the experimental conditions can be found in Table 4.

2.3. Characterization

Both fresh and used oxygen carrier samples were characterized using different methods. Bulk densities of fresh and used particles were measured according to ISO standard 3923–1 by pouring the material into a cylinder of defined volume (25.092 cm^3) through a funnel and weighing the mass of particles in the cylinder. The density measurement was repeated 5 times for each sample. As an indicator of the attrition and agglomeration of the particles during the operation, the particle size distribution of the fresh and used particles was obtained by sieving the particles in the range of 45, 90, 125, 180, 212 and 250 μm.

The outlet streams of the AR and FR were filtered to trap and collect the fines formed during the operation. Given the total hours of operation, the attrition rate of the oxygen carriers was calculated as the rate of the weight loss of in the form of fines per hour of operation with gas fuel, divided by the initial weight of the particles loaded into the reactor [41].

Semiquantitative X-ray powder diffraction (XRD, Bruker D8 DISCOVER) was used to identify crystalline phases in both fresh and used oxygen carrier samples. Scanning electron microscopy with energy dispersive X-ray spectroscopy (SEM-EDX, FEI ESEM Quanta 20) was used to analyze the morphology and chemical composition of the particle.

2.4. Data evaluation

2.4.1. Fuel conversion in 300 W reactor

The fuel conversion in the 300 W reactor is assessed with the CO_2 yield γ_{CO_2}, as shown in Equation (1), which is the ratio of CO_2 volumetric concentration over all the carbon species', i.e. CH_4, CO and CO_2, measured in the outlet gas of FR.

Table 3
Test matrix with different fuels.

Batch	Campaign	Solids inventory, initial	CLOU	→	Fuel		→	CLOU	→	Fuel
1	$CaMnO_3$ – Syngas	300 g	×		850 °C 915 °C Syngas: 2 h	CLOU→Syngas CLOU→Syngas		–		–
2	$CaMnO_3$ – CH_4	300 g	×		850 °C 900 °C 925 °C 950 °C CH_4: 4.5 h	CLOU→CH_4 CLOU→CH_4 CLOU→CH_4 CLOU→CH_4		×		950 °C CH_4: 24.5 h

× : experiment performed; –:experiment not performed.

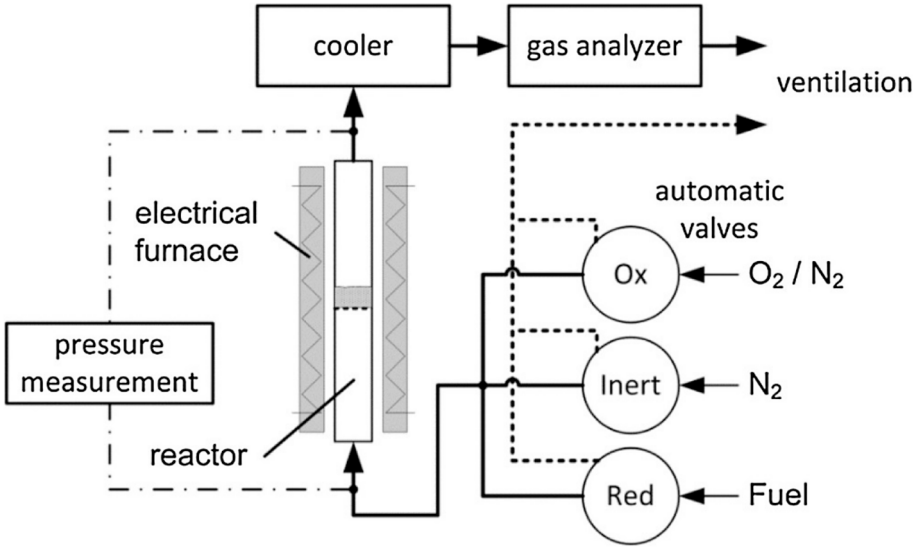

Fig. 5. Schematic illustration of the batch fluidized-bed reactor system[39,40].

Table 4
Experimental scheme of batch reactor tests.

Bed material	Sample weight (g)	Test	Oxidation gas	Inert gas	Reducing gas	F_{ox} (mL_n/min)	F_{inert} (mL_n/min)	F_{red} (mL_n/min)	t_{ox} (s)	t_{inert} (s)	t_{red} (s)	T (°C)	No. of cycles
Silica sands	15	CLOU	5 % O_2	N_2	–	900	600	–	300	600	–	850–950	4
		CH_4	5 % O_2	N_2	CH_4	900	600	450	300	90	20	850–950	8
Fresh sample	15	Activation	5 % O_2	N_2	Syngas	900	600	450	600	90	20	850	4
		CLOU	5 % O_2	N_2	–	900	600	–	600	1000	–	850–950	20
		CH_4	5 % O_2	N_2	CH_4	900	600	450	600	90	20	850–950	20
Fresh sample	2	Activation	5 % O_2	N2	Syngas	900	600	450	600	90	20	850	4
		Syngas	5 % O_2	N_2	Syngas	900	600	900	600	90	20	850–950	20
Used sample	15	Activation	5 % O_2	N_2	Syngas	900	600	450	600	90	20	850	4
		CLOU	5 % O_2	N_2	–	900	600	–	600	1000	–	850–950	12
		CH_4	5 % O_2	N_2	CH_4	900	600	450	600	90	20	850–950	12
Used sample	2	Activation	5 % O_2	N_2	Syngas	900	600	450	600	90	20	850	4
		Syngas	5 % O_2	N_2	Syngas	900	600	900	600	90	20	850–950	20

Note: The abbreviations ox and red denote oxidation and reduction. Flows are normalized.

$$\gamma_{CO_2} = \frac{[CO_2]_{FR}}{[CO_2]_{FR} + [CO]_{FR} + [CH_4]_{FR}} \quad (1)$$

2.4.1.1. Reactivity in batch reactor. The reactivity of oxygen carriers towards gas fuels in the batch reactor is quantified similarly as in 300 W reactor by the fuel conversion. Methane conversion and the CO conversion to CO_2 for the syngas experiments are by Equation (2) and (3),

$$\gamma_{CH_4} = \frac{p_{CO_2}}{p_{CO_2} + p_{CO} + p_{CH_4}} \quad (2)$$

$$\gamma_{syngas} = \frac{p_{CO_2}}{p_{CO_2} + p_{CO}} \quad (3)$$

where p_{CO_2}, p_{CO} and p_{CH_4} are the outlet partial pressures of species CO_2, CO and CH_4.

The conversion of the oxygen carrier is defined according to Equation (4),

$$\omega_i = \frac{m_i}{m_{ox}} \quad (4)$$

where m_i is the mass of the oxygen carrier at time i, and m_{ox} is the mass of the fully oxidized oxygen carrier, which is the mass of the oxygen carrier particles added to the reactor, i.e. 15 g for the oxygen release tests and CH_4 tests, 2 g for the syngas tests.

ω_i can also be calculated as a function of time for oxygen uncoupling, methane and syngas tests as shown in Eqs. (5)–(7) based on mass balances.

$$\omega_{i,CLOU} = \omega_0 - \int_{t_0}^{t_i} \frac{\dot{n}_{out} M_o}{m_{ox} p_{tot}} \left(2p_{O_2,OC}\right) dt \quad (5)$$

$$\omega_{i,CH_4} = \omega_0 - \int_{t_0}^{t_i} \frac{\dot{n}_{out} M_o}{m_{ox} p_{tot}} \left(2p_{O_2,OC} + 4p_{CO_2} + 3p_{CO} - p_{H_2}\right) dt \quad (6)$$

$$\omega_{i,syngas} = \omega_0 - \int_{t_0}^{t_i} \frac{\dot{n}_{out} M_o}{m_{ox} p_{tot}} \left(2p_{O_2,OC} + 2p_{CO_2} + p_{CO} - p_{H_2}\right) dt \quad (7)$$

where $\dot{n}_{out}$ is the molar flux of the dry flue gas and M_o is the molar mass of atom oxygen. $p_{O_2,OC}$ is the outlet partial pressure of oxygen released from the oxygen carrier. p_{H_2} is the outlet partial pressure of hydrogen.

3. Results and discussions

3.1. Experiments in 300 W unit

3.1.1. CLOU effect

Fig. 6 illustrates the CLOU effects, specifically the O_2 released into the inert atmosphere of the FR, at various temperatures for the two batches of calcium manganite particles – one batch for syngas operation

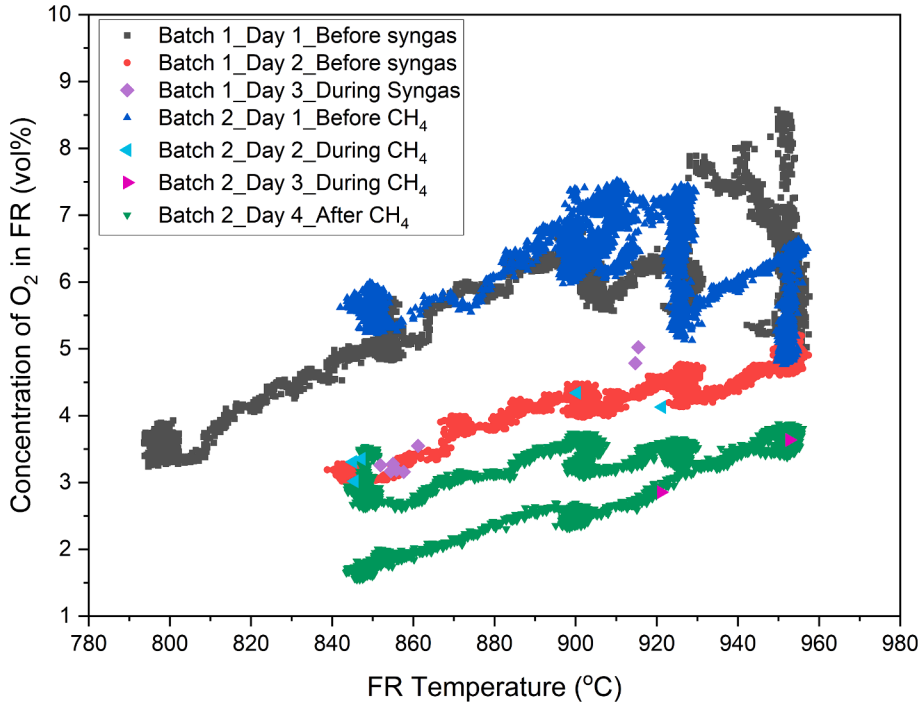

Fig. 6. CLOU effect of calcium manganite oxygen carriers expressed as O_2 released into inert atmosphere of FR under continuous circulation at varied FR temperatures.

and the other for CH_4 operation. The CLOU effects were measured before, in-between and after the fuel tests. For the measurements before and after the operation with syngas and CH_4, the reactors are under CLOU conditions with stepwise increase of temperature. In-between the fuel tests at different temperatures, the CLOU effects were measured before initiating the fuel operation under a given temperature, as shown in Table 3. The data points showing the CLOU effect measured in-between fuel operations in Fig. 6 represent average values.

As presented in Fig. 6, the volumetric O_2 concentrations on Day 1 for both batches are similar, ranging from 3 vol% to 8 vol%, and are notably higher than those on Day 2, 3, and 4. The oxygen deficiency, i.e., δ in $CaMnO_{3-\delta}$, of fresh calcium manganite sample for Day 1 is low, leading to a higher O_2 concentration in the FR. As δ of the steady-state calcium manganite increases with rising temperature [34,42], after the CLOU test with an increase in temperatures on Day 1, δ stabilizes at a higher level. This higher oxygen deficiency in the oxidized calcium manganite

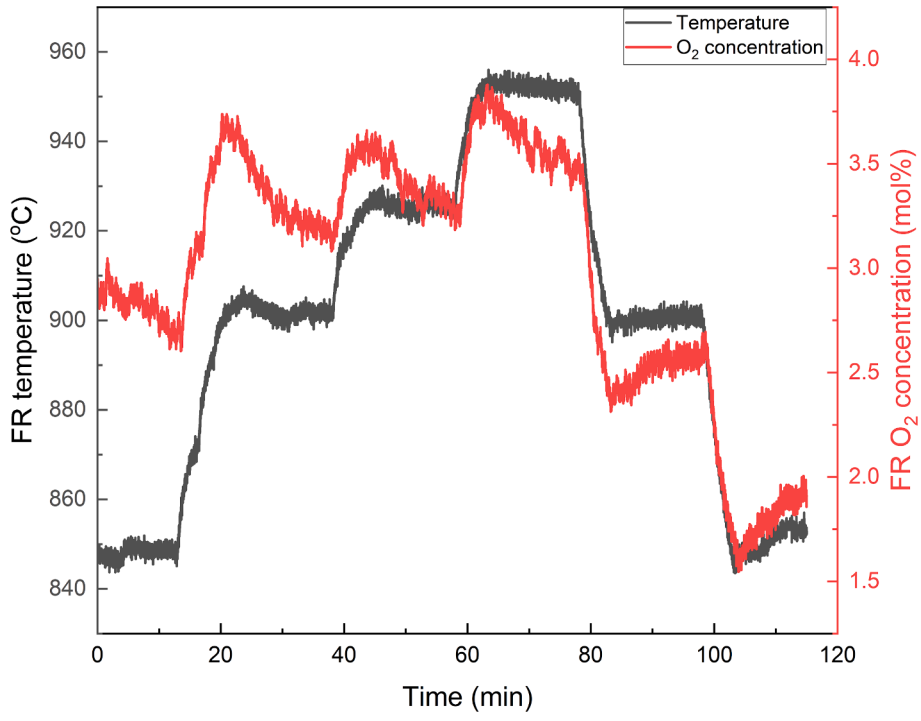

Fig. 7. Change of FR O_2 concentration and temperature over time during the CLOU effect measurements on Day 4 of batch 2.

for Day 2, 3 and 4 could be a potential reason for the discrepancy in O_2 concentration compared to Day 1. A possible explanation would be that the oxygen deficiency is reduced during the slow cooling in the oven after heat treatment, whereas the oxygen carrier tested on Day 2——4 was cooled more rapidly in the 300 W unit. Another possible reason is the decrease of bed height in FR, which would be linked to lower bed height in AR, thus giving lower circulation rate.

In general, the O_2 concentration in the FR increases with rising temperatures, as presented in Fig. 6. The O_2 release in the FR depends on the difference in oxygen deficiency of $CaMnO_{3-\delta}$ in the AR and FR, i.e. $\Delta\delta_{FR-AR}$. At higher temperatures, $\Delta\delta_{FR-AR}$ becomes larger [43], resulting in more O_2 being released in the inert atmosphere of the FR. A similar trend regarding the CLOU effect in the batch reactor was observed, as presented in Fig. 12.

Fig. 7 shows both the increase and decrease of FR temperature over the period for the CLOU effect measurements on Day 4 for batch 2, i.e. green symbols in Fig. 6. In addition to the slow fall in O_2 concentration after each temperature rise and increase in O_2, the opposite behavior is seen after every temperature decrease, first a rapid fall in O_2 concentration and then a gradual increase. Temperature may influence solids circulation rates, the oxidation and O_2 release rates of the oxygen carriers, but more importantly the equilibrium amount of oxygen in the particle for a given O_2 partial pressure over particles. When the temperature rises, the steady-state of $CaMnO_{3-\delta}$, is characterized by an increased δ [34,42], and thus the excess oxygen will be released from calcium manganite. Hence, a temperature increase will first cause a release of O_2, and as the steady state δ value is approached, O_2 will fall. Comparing the temperature increase and decrease in Fig. 6 of Day 4, green line, and the curve versus time in Fig. 7, clearly indicates that steady state of calcium manganite were not reached neither during increase nor during decrease. Consequently, the steady state should be in between the green upper line indicating temperature increase and the green lower line indicating temperature decrease.

The relatively lower O_2 concentrations on Day 3 and 4 of Batch 2 compared to those on Day 2, 3 of Batch 1 and Day 2 of Batch 2 as presented in Fig. 6, are to a large part explained by a 25 % increase in gas flow, resulting from increasing argon flow for the upper loop seal from 0.212 to 0.512 L_n/min. It is evident that calcium manganite releases O_2 in FR with O_2 concentrations ranging from 2 vol% to 8 vol%, although the higher ranges in concentration are undoubtedly not relevant for steady-state conditions. Rydén et al [11,44], reported similar levels of oxygen release with $CaMn_{0.875}Ti_{0.125}O_3$ which was synthesized by spray drying using standardized aqueous solutions, using an earlier design of the same 300 W CLC reactor. From these CLOU effect tests, it is quite clear that the simple mixing and calcination of manganese ore and limestone have resulted in an oxygen carrier with good ability to release oxygen to the gas phase.

3.1.2. *Reactivity towards syngas and CH_4*

The reactivity of calcium manganite towards syngas and CH_4 was investigated in the 300 W CLC unit at different fuel flowrates and temperatures, as summarized in Fig. 8. Here, the variations in fuel flow are expressed as the ratio of the bed mass in the fuel reactor to thermal power of the fuel flow. In total, 31 h of CLC operation with fuels were conducted in the 300 W unit, including 2 h with syngas and 29 h with CH_4.

In general, the CLC operations with syngas and CH_4 proceeded smoothly and showed high repeatability. Tests carried out with syngas at 850 °C and 915 °C, as indicated by filled and empty red circles respectively in Fig. 8, showed complete syngas conversion, even at low temperatures and low fuel reactor bed mass over fuel ratios. For instance, full syngas conversion is achieved at 850 °C with high fuel flow, corresponding to a fuel reactor bed mass/fuel power ratio of 200 kg/MW_{th}. Out of 18 tested manganese ores used in the same, or previous versions of the 300 W unit, only one, known as UMK, demonstrated a syngas conversion as higher 95 % under similar operating conditions [2].

Various parameters were investigated during experiments with CH_4. The reactivity towards CH_4 was found to improve at higher temperatures. For instance, with a fuel reactor bed mass/fuel power ratio of 400 kg/MW at 850 °C, the CO_2 yield is 61 %. However, the yield is increased to 97 % by raising the temperature to 950 °C, as depicted in Fig. 8. This

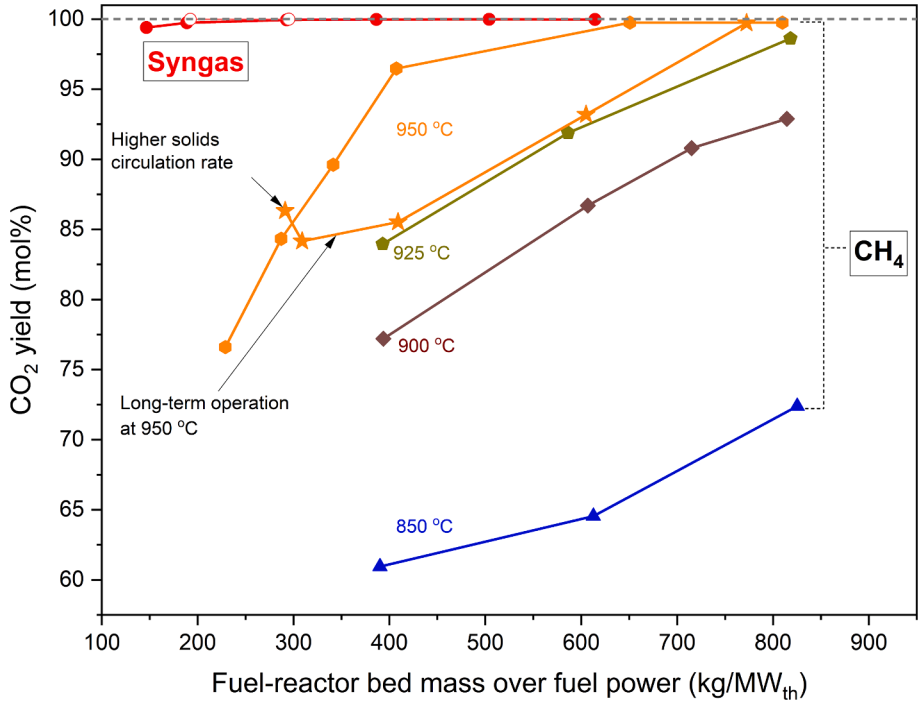

Fig. 8. Conversion of syngas and CH_4 under various temperatures and fuel-reactor bed mass over fuel power ratio in 300 W continuous unit. Filled and empty red circles show conversion of syngas at 850 and 915 °C, respectively. (For interpretation of the references to colour in this figure legend, the reader is referred to the web version of this article.)

improvement aligns with the general principle that chemical reactions proceed faster at elevated temperatures. Additionally, it was observed that CH_4 conversion is enhanced with bed mass/fuel ratio. At 950 °C, gas conversion increases from 77 % to 100 % when the fuel-reactor bed mass to fuel ratio is raised from 200 to 650 kg/MW_{th}. The gas concentrations in the outlet of the FR and AR in the 300 W unit, with varying the CH_4 flowrates from 0.16 to 0.51 L_n/min at 950 °C, are illustrated in Fig. 9. Prior to CH_4 addition, the FR was fluidized with Argon, resulting in O_2 concentrations around 18.2 vol% in the AR and 3.6 vol% in the FR, as indicated in the first 6 min of data in Fig. 9. Upon CH_4 introduction to the FR, AR-O_2 gradually decreased, and FR-CO_2 increased with rising CH_4 flowrates. Full gas conversion was achieved during the first two CH_4 operation periods corresponding to the two orange hexagon symbols on the far right at 950 °C in Fig. 8, showing some remaining O_2 in the FR outlet. Starting from the third CH_4 operation period, unconverted CH_4 was observed in the FR outlet, and in the last operating period, around 0.4 vol% CO was detected in the FR outlet.

Ilmenite was tested with natural gas in the 300 W unit, albeit a previous design of the reactor, achieving 65 % to 82 % gas conversion, with a natural gas flowrate ranging from 0.37 to 0.16 L_n/min at 950 °C [45]. In comparison, calcium manganite, tested under similar conditions with CH_4 as the fuel in this study, demonstrated gas conversions from 90 % to 100 %. Among the 18 manganese ores tested previously, including the Eramet HM manganese ore used in producing calcium manganite in this work, the highest CH_4 conversion was 82 % with UMK at 950 °C with fuel reactor bed mass as 420 kg/MW_{th} [2]. However, under similar conditions, the calcium manganite in this study can achieve 96 % CH_4 conversion. Another perovskite-structured oxygen carrier, $CaMn_{0.875}Ti_{0.125}O_3$, produced by spray pyrolysis using standardized aqueous solutions, achieved a 95 % conversion of natural gas in a similar 300 W unit with FR bed mass set at 1000 kg/MW_{th} at 950 °C [11]. 7 out of 8 different $CaMn_{0.9}Mg_{0.1}O_{3-\delta}$ and $CaMn_{0.775}Mg_{0.1}Ti_{0.125}O_{3-\delta}$ produced from different manganese oxides and titanium oxides raw materials with higher purities exhibit relatively higher CH_4 conversion, ranging from 90 % to 100 %, with fuel reactor bed mass over fuel power ratio ranging from 380 to 600 kg/MW_{th} at 900 °C in the same reactor system compared to the calcium manganite studied in this work, which shows 77 % to 87 % under similar conditions [46]. However, at 950 °C, calcium manganite in this work achieves similar CH_4 conversion to 3 out of 5 tested $CaMn_{0.775}Mg_{0.1}Ti_{0.125}O_{3-\delta}$, all of which achieve above 95 % CH_4 conversion with FR bed mass over fuel power ratio ranging from 400 to 600 kg/MW_{th}, outperforming the remaining 2 samples [46].

Towards the end of the experimental campaign with CH_4, extended operation at 950 °C at varying fuel flows were conducted, represented by the star-shaped symbols in Fig. 8. Each data indicated by the star symbol is an average value based on 4 to 5 h of continuous operation with CH_4 at a constant temperature and fuel flow, except for the last one to the left, indicated with a higher solids circulation rate. When the fuel flow is small or the FR bed mass over fuel ratio is large, such as the first star symbol to the right, the results based on a 5- hour period are similar to those based on a short period, around 15 min. However, with an increase in fuel flow, these long-term operation results give lower CO_2 yields compared to those with short operation periods. During the 4 to 5 h of CH_4 operation, CO_2 yields decreased over time, which could potentially be explained by a decrease in reactivity of calcium manganite or a decrease in solids circulation caused by e.g. fines accumulation in the top part over the reactor. Fig. 10 shows the change of CH_4 conversion and FR bed mass over fuel power over the 4 to 5 h extended periods with average FR bed mass over fuel power as 773 and 309 kg/MW_{th}. When fuel flow is lower, i.e. the FR bed mass over fuel power is 773 kg/MW_{th}, the CH_4 conversion stays at 100 %, even though there is a slight decrease of the FR bed mass. When the fuel flow is higher, i.e. the FR bed mass over fuel power is 309 kg/MW_{th}, a gradual decrease of both CO_2 yield and FR bed mass over fuel ratio over time can be observed from Fig. 10. Increasing the solids circulation rate by raising the air flow in AR from 8 to 9 L_n/min showed improved gas conversion, which can be indicated by the star symbol to the left in Fig. 8 and the black lines in Fig. 10.

3.1.3. Attrition rate

The mass of fines collected in the filters for AR and FR flue gases and the water seal of FR has been systematically recorded to monitor the attrition of calcium manganite in the 300 W unit. Fig. 11 shows the light microscope images of fines collected from the AR filter, of which the

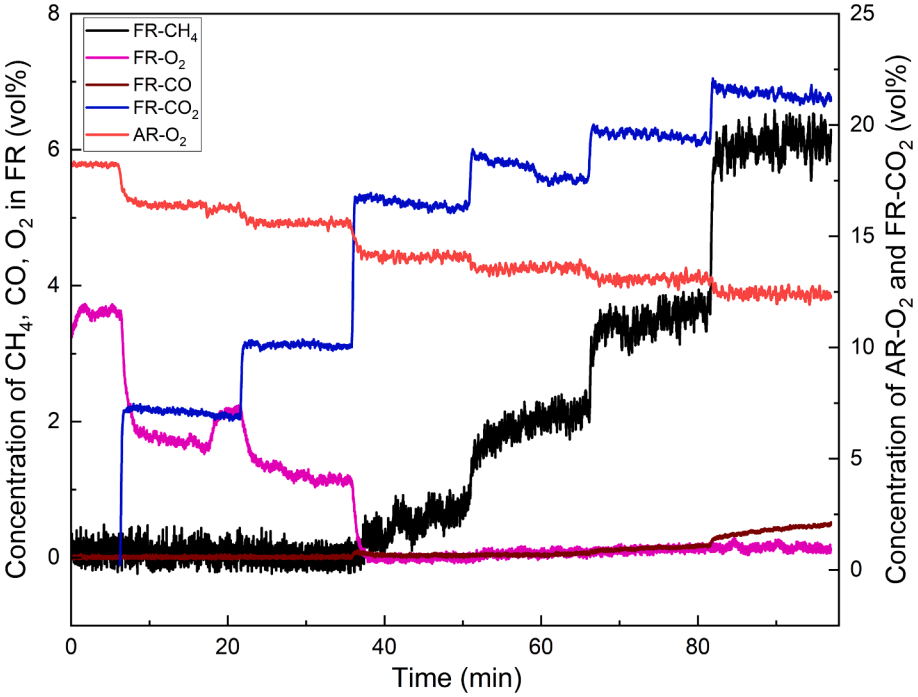

Fig. 9. Gas concentrations during the tests of calcium manganite at T_{FR}=950 °C with 0.16–0.51 L_n/min CH_4 in 300 W unit. The balance is argon, which was used to fluidize the loop-seals. The AR was fluidized with 8 L_n/min air.

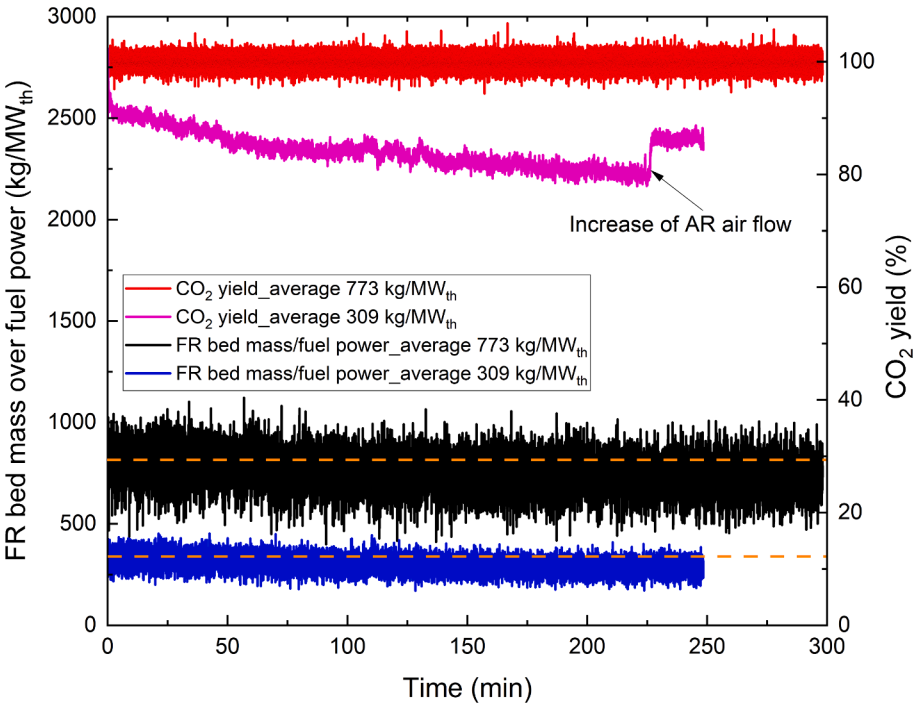

Fig. 10. Conversion of CH_4 and FR bed mass over fuel power over 4–5 h continuous operations with average FR bed mass over fuel power as 773 kg/MW_{th} and 309 kg/MW_{th} at 950 °C.

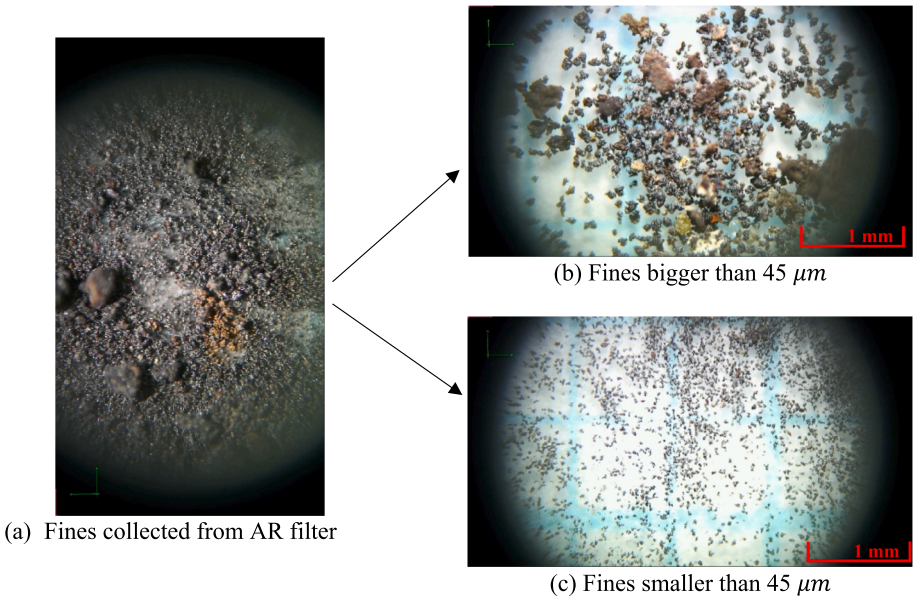

(a) Fines collected from AR filter

(b) Fines bigger than 45 μm

(c) Fines smaller than 45 μm

Fig. 11. Light microscope images of fines collected from the AR filter of 300 W system after the experimental campaign with CH_4.

majority of the particles were smaller than 45 μm, i.e. 86 wt% of the mass of fines collected.

In Table 5, it can be observed that the attrition of the calcium manganite oxygen carrier is higher with syngas (1.0 %) compared to CH_4 (0.1–0.3 %). Rydén et al., described two types of oxygen carrier attrition during CLC in circulating fluidized beds, including the mechanical attrition caused by fluidization itself and attrition due to property changes originating from thermal shock, internal gas pressure and chemical reaction [38]. The attrition rate of calcium manganite with syngas is around 1.0 wt%/h based on 2 h operation. Whereas the calcium manganite particles with CH_4 exhibit an attrition rate of 0.27 wt %/h based on 8 h operation with CH_4. It is expected the attrition rate decreases with increased time of operation. Therefore, the attrition rate based on the first 2 h of operating with syngas should be higher than the one based on the first 8 h of operating with CH_4.

The Eramet HM manganese ore used for producing calcium manganite in this study experiences an attrition rate ranging from 0.09 to 0.71 wt%/h in the same 300 W system [2]. In comparison, $CaMn_{1-x-y}Mg_xTi_y$, produced from higher-purity raw materials by spray drying, undergoes attrition rates ranging from 0.03 to 0.13 wt%/h [47]. However, in the current study, calcium manganite experiences average attrition rates ranging from 0.15 to 1.03 wt%/h with syngas and CH_4. This higher attrition rate could be attributed to the rounding effect observed on the first day of the operation.

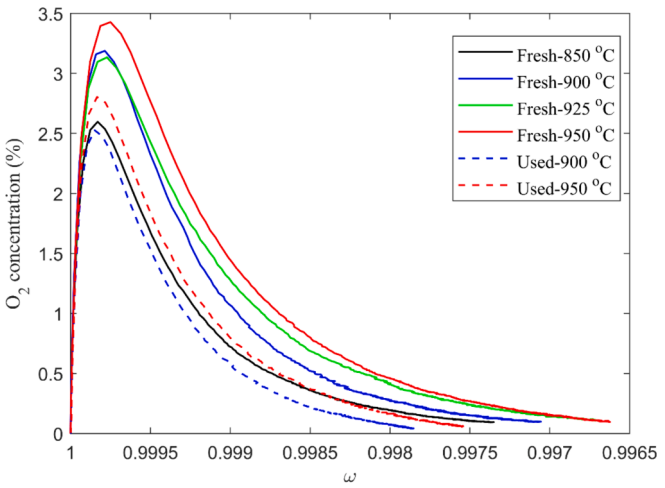

Fig. 12. Oxygen release in an inert atmosphere of the batch reactor as a function of conversion of 15 g calcium manganite oxygen carrier under various temperatures. (Fresh: averaged data based on 5 cycles; Used: averaged data based on 3 cycles, sampled after 29 h operation with CH_4 in 300 W unit.).

3.2. Experiments in batch reactor

3.2.1. O_2 release

The oxygen release of fresh and used calcium manganite samples was further examined at varying temperatures in a batch fluidized-bed reactor. Fig. 12 illustrates the O_2 concentrations in an N_2 atmosphere, with the ones from blank tests subtracted, versus the conversion of 15 g fresh and used calcium manganite samples at different temperatures. It is evident that the oxygen release improves with the rising temperature, consistent with the results regarding the CLOU effect in the 300 W circulating fluidized-bed reactor. The amount of O_2 released is higher, and the speed of release is faster at higher temperatures. This corresponds to the decrease in the finally obtained ω, from 0.9973 at 850 °C to 0.9967 at 950 °C, implying that 0.27–0.33 wt% of the mass of oxygen carrier could be released as O_2 in an inert atmosphere at 850 and 950 °C.

Furthermore, it can be also seen from Fig. 12 that the oxygen uncoupling ability of the used sample is inferior to that of the fresh sample. At 950 °C, 0.24 wt% of the used sample is released as O_2, which is lower than the 0.33 wt% for the fresh sample. This could be attributed to the decrease in active compounds for O_2 uncoupling. It has been reported that $CaMnO_3$ might decompose to Ca_2MnO_4 and $CaMn_2O_4$ at high temperatures in some references, affecting the full reoxidation in the AR [11,24,33,34]. Although the phase Ca_2MnO_4 was not found in fresh or used samples, it is possible that there is less active compound in the used samples due to the decrease of the relative ratio of perovskite-structured $CaMnO_3$ over marokite $CaMn_2O_4$ in used samples compared to the fresh one, as described in sections 3.3.2 and 3.3.3. Another potential reason is the smaller sizes, higher density, and sphericity of the used particles, as presented in Fig. 3 and Table 6, resulting in more compact particles and a lower specific surface area. A calculation of the expected change in $\Delta\delta$ at equilibrium at 900 °C with oxygen partial pressure going from 5 % O_2 to 0.1 % O_2 [43], indicates that the change in mass-based conversion, i.e. $\Delta\omega$, should be 0.007 whereas it is 0.003 in the batch reactor test as presented in Fig. 12.

3.2.2. Reactivity towards CH_4

Fig. 13 presents an example of the average flue gas concentration profile of the methane cycles with the fresh calcium manganite sample. At 0 s, 5 % O_2 was switched off, and N_2 was injected for 90 s. The O_2 concentration in Fig. 13 only considers the O_2 released from the calcium manganite particles, i.e. O_2 concentration from blank tests with silica sands is subtracted. At the end of the inert period, there is around 1.1 % of O_2 resulting from the O_2 uncoupling behavior of the oxygen carrier. At 90 s, N_2 flow was turned off, and CH_4 was switched on for 20 s. The peaks of different gases, i.e. CO_2, CO, CH_4 and H_2, do not show up until about 120 s due to the time delay in the system. CO and H_2 are generated from the reforming of CH_4. The initial H_2 peak, however, is most likely an artifact, associated with the difficulties in measuring and compensating for other gases under transient conditions. Flushing with N_2 after the reduction period starts at 110 s. When the flushing ends at 200 s, the reoxidation with 5 % O_2 will take place, not shown in Fig. 13.

Fig. 14 illustrates the conversion of oxygen carrier samples during this 200 s cycle with CH_4 at varying temperatures. O_2 is released from the oxygen carrier in the inert period and detected after approximately 20 s when the oxidation atmosphere is switched to N_2. At around 120 s, the calcium manganite samples started to be converted quickly. Because of more rapid conversion, the reduction degree of calcium manganite samples increased with temperature, i.e. increase of $\Delta\omega$ from 0.5 % at 850 °C to 1.5 % at 950 °C. The reduction degree of the used samples is slightly higher than that of the fresh sample at the lower temperatures, whereas the difference is insignificant at higher temperatures.

Fig. 15 depicts the CH_4 conversion versus the mass-based conversion of both fresh and used calcium manganite samples at various temperatures. Highest CH_4 conversion varies from 46 % to over 95 % depending on temperature. Elevated temperatures significantly enhance CH_4 conversion. Notably, there is little difference in reactivity between the fresh and used samples, particularly at higher temperatures, despite the higher O_2 release of the fresh samples under inert conditions. This contrasts with the discernible difference in O_2 release between the fresh and used samples. However, the reactivity of the CLOU oxygen carriers does not solely depend on the amount and rate of oxygen release. This is because CH_4 conversion in the fuel reactor can occur through two pathways: direct oxidation of CH_4 by the oxygen carrier or by the

Table 6
Physical properties of fresh and used calcium manganite samples.

Oxygen carrier sample	Bulk density (kg/m^3)	Crushing strength (N)	Size distribution D_{10}, D_{50}, D_{90} (μm)	Attrition index measured in a jet-cup attrition rig (wt%/h)
Fresh_$CaMnO_{3-\delta}$	1102	2.87	112, 157, 244	4.6
Used_$CaMnO_{3-\delta}$_Syngas	1231	1.07	74, 85, 185	7.2
Used_$CaMnO_{3-\delta}$_CH_4	1304	1.17	84, 129, 202	5.0

Table 5
Attrition of calcium manganite in 300 W unit.

Initial OC load (g)	Test	Common filter (g)	AR filter (g)	FR filter (g)	FR water seal (g)	Total loss (g)	Fuel operation time (h)	Attrition (wt %/h)	Average attrition (wt %/h)
300	Syngas_Day 3	4.8	1.3	0.1	–	6.2	2	1.03	1.03
300	CH_4_Day 2,3,4	2.0	0.6	0.2	3.7	6.5	8	0.27	0.15
	CH_4_Day 5	0.0	0.1	0.0	1.7	1.8	5	0.12	
	CH_4_Day 6	0.0	0.3	0.1	1.0	1.4	5	0.09	
	CH_4_Day 7,8	0.1	0.3	0.1	0.6	1.1	5.6	0.07	

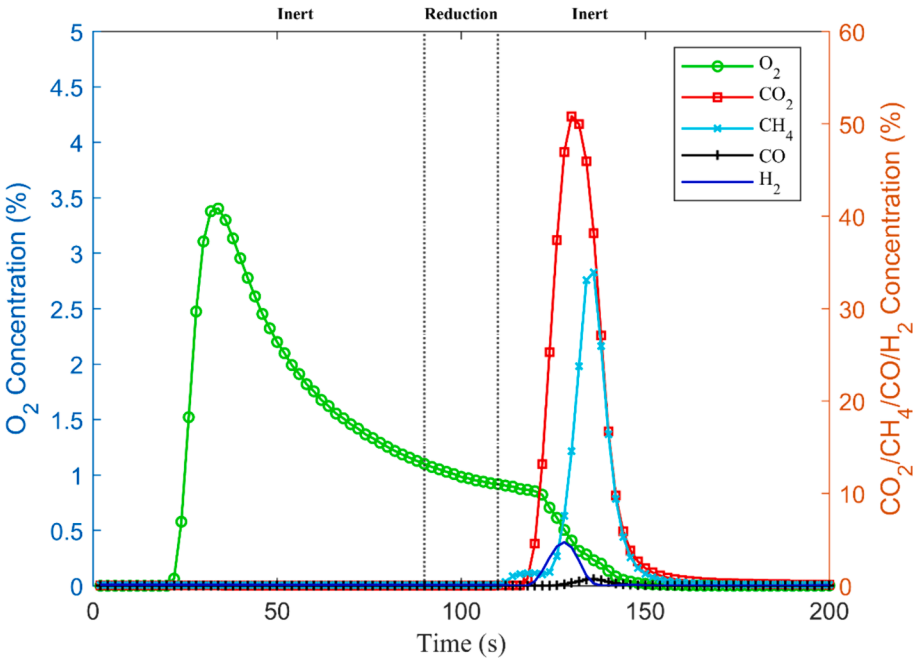

Fig. 13. Average gas concentrations of the methane cycles as a function of time at 950 °C with the fresh calcium manganite sample.

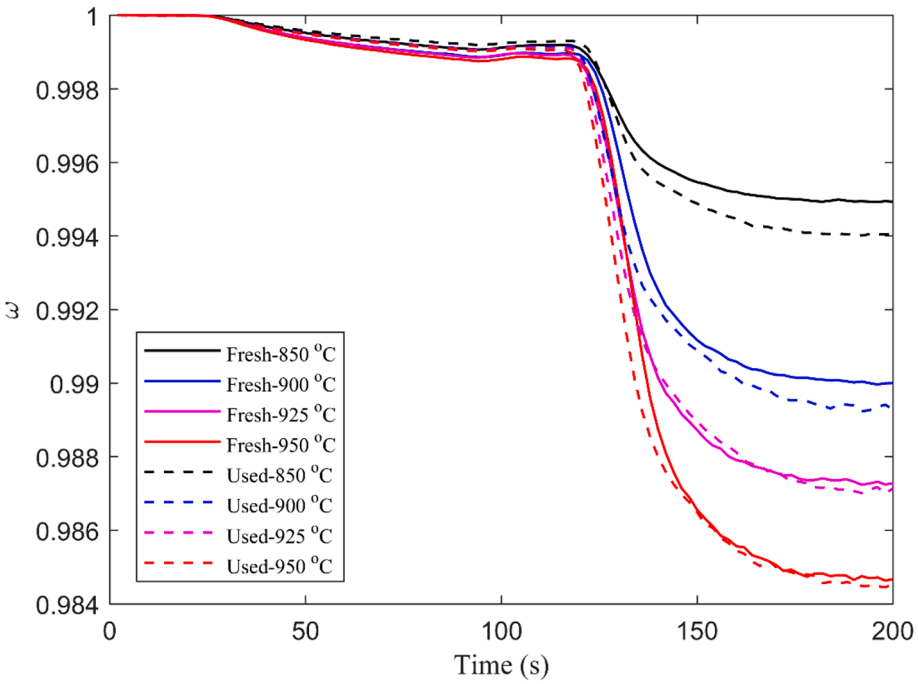

Fig. 14. Conversion of fresh and used calcium manganite samples over time with CH_4 in the batch reactor at varying temperatures.

molecular oxygen released from the oxygen carriers. The CH_4 conversion generally decreases with increasing reduction degree of calcium manganite particles.

3.2.3. *Reactivity towards syngas*

Fig. 16 presents an example of the average flue gas concentration profile of the syngas cycles with the fresh calcium manganite sample. A 2 g calcium manganite sample was mixed with 13 g silica sand for the syngas test. The switches of the inert and reduction periods for syngas tests are similar to methane tests. The O_2 release of the 2 g oxygen carrier sample in the first inert period is almost completed in 90 s.

Fig. 17 illustrates the conversion of oxygen carrier samples during this 200 s cycle with syngas at varying temperatures. The conversion of the calcium manganite samples was deeper reaching a $\Delta\omega$ of 7.5 %, which is higher compared to methane reaching $\Delta\omega$ of 1.5 %. This difference is an effect of differences in the amount of sample, the reduction capacity of the gas as well as the actual gas conversion. Unlike the reactions between calcium manganite and methane, the reactions with syngas are less sensitive to temperature. Moreover, no significant difference between used and fresh samples was seen.

Fig. 18 depicts the syngas conversion versus the conversion of both fresh and used calcium manganite samples at different temperatures.

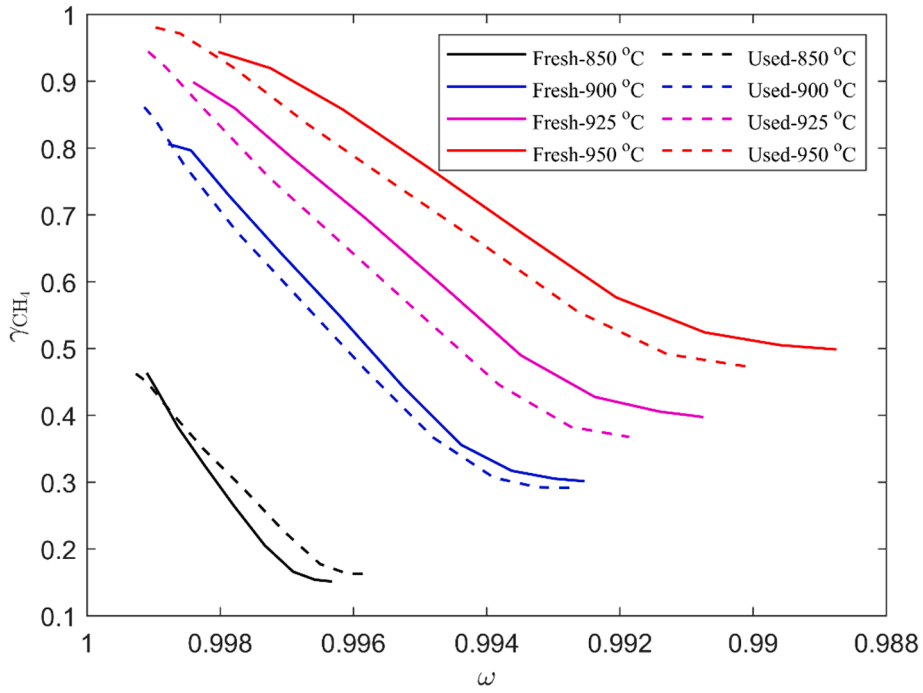

Fig. 15. Methane conversion over the corrected conversion of fresh and used calcium manganite samples at varying temperatures in the batch reactor.

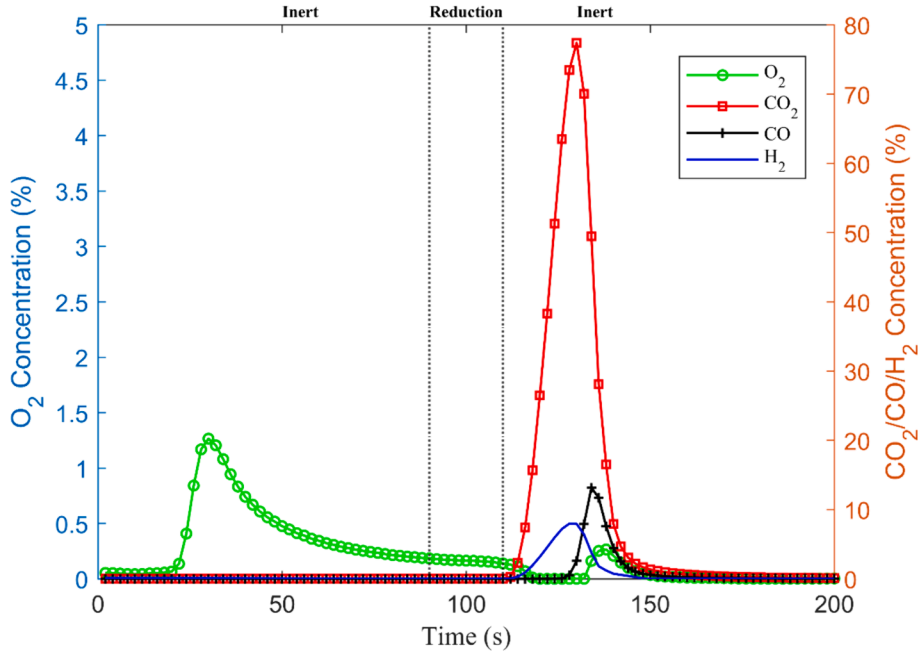

Fig. 16. Average gas concentrations of syngas cycles as a function of time at 950 °C with the fresh calcium manganite sample.

With the exception of 850 °C, all calcium manganite samples achieve full syngas conversion for ω ranging from 1 to 0.99. As reduction progresses, less oxygen becomes available in the oxygen carrier, leading to decreased reactivity. This results in a decline in syngas conversion at higher reduction of the oxygen carrier samples. Similar to their reactivity towards CH_4, the reactivity of the fresh and used calcium manganite samples towards syngas is almost identical, despite the fresh sample exhibiting higher O_2 release in inert atmosphere as shown in Fig. 12. As in the case of CH_4, the reactivity of CLOU materials does not solely depend on the amount and rate of oxygen release by the oxygen carriers. The temperature has no significant impact on the performance, except for lowest temperature of 850 °C, where fresh sample shows lower gas conversion at the reduction phase with ω from 0.99 to 0.95.

3.3. Characterizations

3.3.1. Physical properties

The calcium manganite particles exhibited good fluidization characteristics throughout the experiments. After operations with syngas and CH_4 for 2 h and 29 h, respectively, the used particles have approximately 12 % and 18 % higher density than the fresh one as shown in Table 6. The size distributions of the used samples appear to shift towards smaller

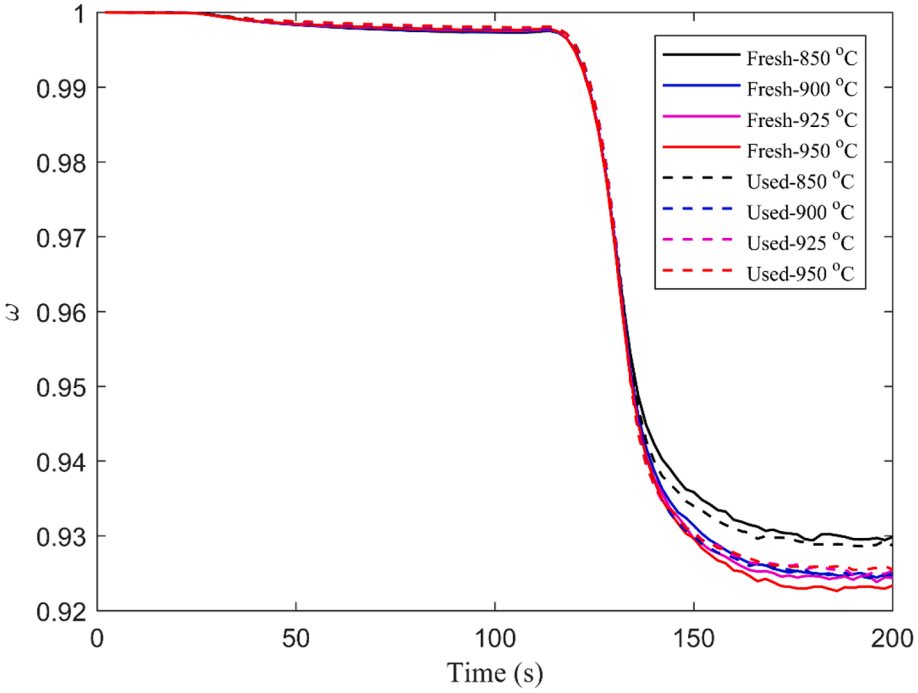

Fig. 17. Conversion of fresh and used calcium manganite samples over time with syngas in the batch reactor at varying temperatures.

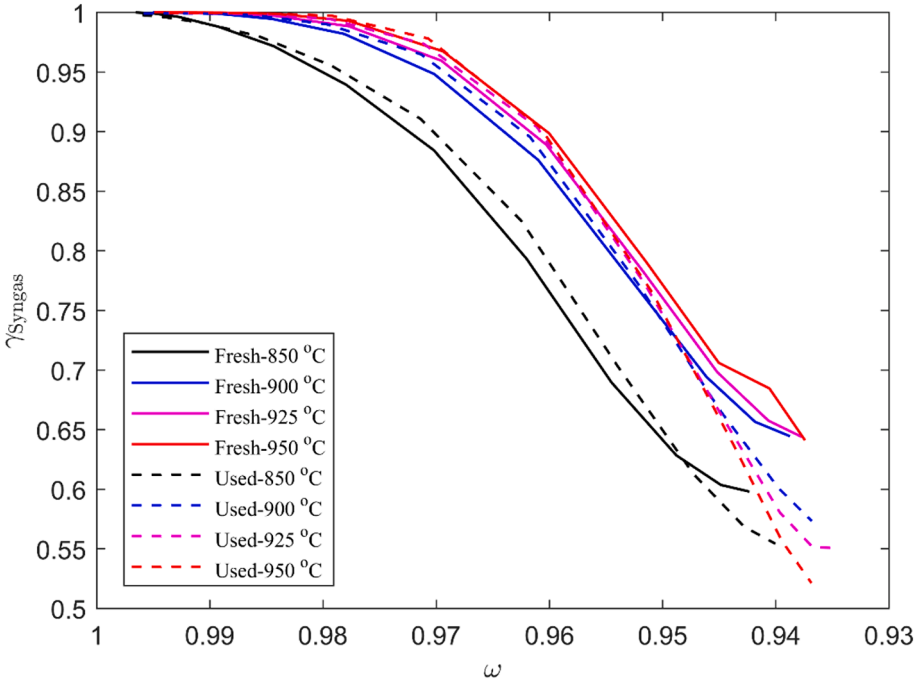

Fig. 18. Syngas conversion over the corrected conversion of fresh and used calcium manganite samples at varying temperatures in the batch reactor.

sizes compared to the fresh ones. This suggests that the particles break into smaller ones during the operations with fuels, likely attributed to the irregular shapes of the fresh particles and the chemical reactions with fuels.

The attrition index measured in the attrition rig is significantly larger than the estimated attrition in the 300 W unit, as indicated in Table 5. Furthermore, the attrition rate decreases with the increase of operational time with CH_4, and the primary attrition occurs in the initial hours of operation with fuel in the 300 W unit. This implies that the used sample should logically have a lower attrition rate compared to the fresh one. However, the crushing strength of the used samples is smaller than that of the fresh sample, and furthermore the attrition index measured in the jet-cup attrition rig is slightly larger after 29 h of operation. As previously noted, there is, however, no strong correlation among the commonly used crushing strength index, attrition index measured in a jet-cup attrition rig, and the estimated attrition in 300 W unit [2,38].

3.3.2. *Crystalline phase analysis*

Two main crystalline phases, i.e. $CaMnO_3$ and $CaMn_2O_4$, have been identified in both fresh and used calcium manganite samples based on

the XRD patterns, see Fig. 19. $CaMnO_3$ is the desired product, while $CaMn_2O_4$ is an undesired byproduct that might form during the production process and the CLC operations of these calcium manganite particles. But the properties of $CaMn_2O_4$ as oxygen carrier has not been studied, which means that the implications of formation of $CaMn_2O_4$ are not well known. The relative molar ratio of $CaMnO_3$ to $CaMn_2O_4$ in fresh sample is 3.5, as indicated in Table 7, corresponding to a molar ratio of Ca/Mn in fresh sample as 0.82. As described in section 2.1, a mixture of 69.00 g Eramet HM manganese ore and 55.35 g limestone was used for the production of calcium manganite oxygen carriers, resulting in a molar ratio of Ca/Mn as 0.83. This ratio closely aligns with the one suggested from the content ratio of the two main phases. The presence of $CaMn_2O_4$ in the fresh sample is most likely attributed to the mixing ratio of the raw materials giving a surplus of Mn. However, the impurities in Eramet HM manganese ore might substitute some Mn in the perovskite structure, thus increasing the surplus of Mn. Limited contact between the raw materials during the production process could be an additional reason for the formation of $CaMn_2O_4$. Overall, the production of calcium manganite from manganese ore and limestone appears relatively straightforward and adjusting the mixing ratio of Ca/Mn in the future production process would likely reduce the formation of $CaMn_2O_4$.

As observed in Fig. 19, the heights of the peaks corresponding to the $CaMnO_3$ phase (in relation to those corresponding to $CaMn_2O_4$) in the used samples are generally lower than those in the fresh sample. Removal of 10.8 g out of 300 g with slightly higher Ca/Mn ratio does not explain a 11 % decrease of Ca/Mn in used sample, cf. Fig. 23. There is a decrease in the $CaMnO_3/CaMn_2O_4$ ratio across the fresh, intermediate, and final samples, along with the higher content of $CaMnO_3$ compared to $CaMn_2O_4$ in the fines collected from the AR filter and water seal, as indicated in Table 7. The latter suggests that $CaMnO_3$ is more susceptible to attrition. A possible explanation could be that Ca has not penetrated fully into the Mn particles giving higher $CaMnO_3$ on the surface. However, it should be noted that the XRD is only semiquantitative. Furthermore, the small loss of fines cannot explain the large decrease in $CaMnO_3/CaMn_2O_4$ ratio, which corroborates the suggested higher concentration of $CaMnO_3$ on the surface. Another possible explanation is that the $CaMnO_3$ has become more amorphous, as the detection is dependent on the existence of a crystalline phase.

Table 7
Relative weight percentages of phases in fresh, intermediate and final calcium manganite samples, derived with semi-quantitative analysis of the XRD data.

Phase	Fresh	Intermediate	Final	Fines from AR filter	Fines from water seal
$CaMnO_3$	70 %	60 %	50 %	80 %	70 %
$CaMn_2O_4$	30 %	40 %	50 %	20 %	30 %
Molar ratio of $CaMnO_3$/ $CaMn_2O_4$	3.5	2.2	1.5	6.0	3.5

Note: Intermediate sample is from AR after 5 h test with CH_4. Final sample is from AR after 24 h of operation with CH_4.

3.3.3. Morphology and chemical distribution

The calcium manganite particles exhibit a porous structure, as shown in Fig. 20. The SEM image of fresh calcium manganite particles reveals two distinct zones within the particles, namely a bright zone and a somewhat darker zone. The elemental distribution of Mn through particles highlights these two different zones in fresh calcium manganite, as illustrated in Fig. 21. SEM-EDX analysis indicates the relative contents of Ca, Mn, Fe, and Al in the dark and bright zones, as shown in Fig. 22. The dark zone has a Ca/Mn molar ratio of about 1, indicating $CaMnO_3$. Conversely, the bright zone displays a Ca/Mn molar ratio of approximately 2, corresponding to $CaMn_2O_4$. As discussed in section 3.3.2, the formation of $CaMn_2O_4$ can be explained by the Ca/Mn molar ratio being below 1. A possible additional factor could be the large size of raw material particles, up to 90 μm, giving limited contact between calcium and manganese elements. On the other hand, there are no zones where Ca is missing indicating good penetration despite the large particle size, Fig. 21.

The manganese ore, i.e. Eramet HM, contains 7.1, 4.5, and 1.7 wt% of Fe, Al and Si, as shown in Table 1. Fe substitution of Mn in the perovskite structure of calcium manganite can improve the stability of the microstructure of the particles, the oxygen uncoupling ability, and the reactivity [23,31,48]. Al and Si are mostly seen in inert phases, i.e. with no oxygen transfer capability and calcium silicates and aluminates can be formed when 50 % mixing ratio Ca/(Mn + Fe) is employed for the production of calcium manganite from CaO and Mn ore containing Si and Al [32]. The latter appears to slow down the redox reaction kinetics. Interestingly, XRD analysis of the calcium manganite studied in this

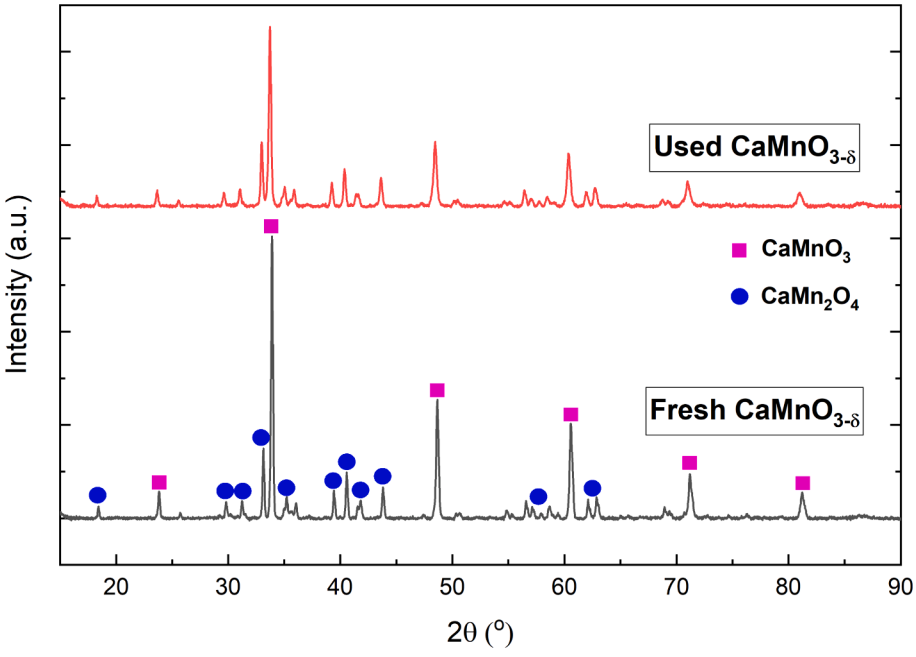

Fig. 19. Crystalline phase analysis of the fresh and used calcium manganite samples.

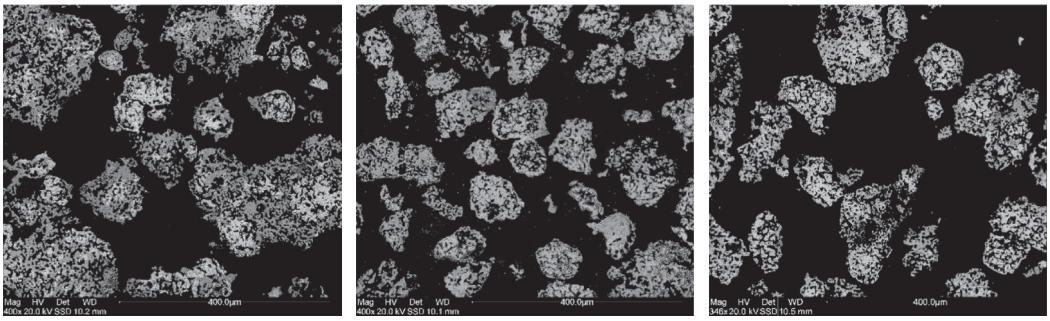

Fig. 20. SEM images of the fresh and used calcium manganite samples.

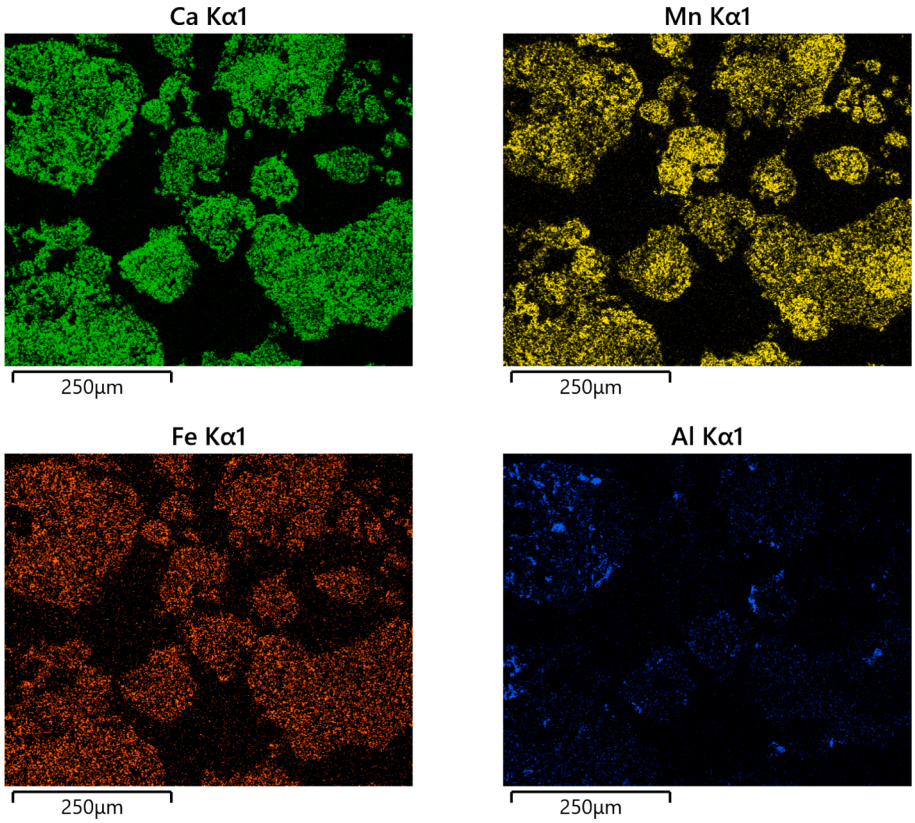

Fig. 21. EDX elemental mapping of fresh calcium manganite particles: Ca, Mn, Fe, Al.

work did not reveal any presence of phases containing Fe, Al and Si. However, SEM-EDX analysis demonstrates that the dark zone, i.e. $CaMnO_3$ zone, contains higher concentrations of Fe, Al and Si, Fig. 22. This suggests that the perovskite structure can incorporate Fe, Al and Si into its structure.

The average contents of various elements in fresh and used samples, along with fines collected from water seal and AR filter, are illustrated in Fig. 23. The fines primarily consist of $CaMnO_3$ as described in section 3.3.2, which is corroborated by the Ca/Mn molar ratio of fines of around 1, as indicated in Fig. 23. In comparison to the fresh sample, the used sample exhibits higher manganese content and lower calcium content, suggesting that $CaMn_2O_4$ persists in the reactor instead of being elutriated as fines. However, the small loss of fines with somewhat higher Ca/Mn ratio cannot explain the change in Ca/Mn ratio between fresh and used particles in Fig. 23.

3.4. Comparisons with other oxygen carriers

The CLOU effect of calcium manganite in this study ranges from 2 vol % to 8 vol% in the 300 W unit, significantly surpassing the CLOU effect of the raw material, Eramet HM manganese ore. The manganese ore exhibited an O_2 release of approximately 0.15 vol% to 0.7 vol% in the outlet of FR in the same unit [2]. This difference is attributed to the transformation of the active phase for O_2 release from Mn_2O_3 in the manganese ore to $CaMnO_{3-\delta}$ in calcium manganite. Another perovskite-structured material, $CaMn_{0.875}Ti_{0.125}O_3$, synthesized by spray drying using standardized aqueous solutions, demonstrates a comparable O_2 release ability, around 4 vol% in the outlet of the fuel reactor in a previous design version of the 300 W chemical-looping combustor [11]. This indicates that calcium manganite produced from natural ores can reach an O_2 release ability comparable to those produced from high-purity raw materials by more complex methods.

The calcium manganite investigated in this study demonstrates complete syngas conversion at relatively low temperature and a low fuel

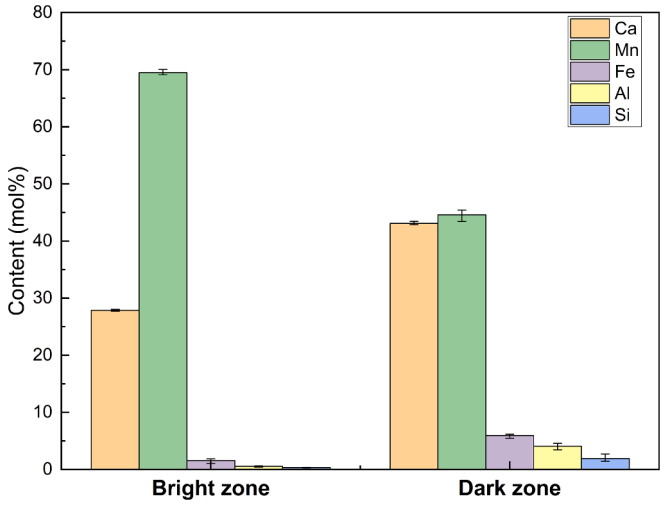

Fig. 22. Relative contents of different elements in the bright and dark zones of the fresh calcium manganite particles.

reactor bed mass-to-power ratio, while the raw manganese ore, Eramet HM, achieves only around 90 % syngas conversion, even with a higher bed mass to fuel ratio [2]. The reactivity of calcium manganite towards CH_4 is also significantly higher than that of Eramet HM. The CH_4 conversion can exceed 95 % for calcium manganite, which is much higher than the 40 % observed for Eramet HM under similar operating conditions, and comparable to the reactivity performance of $CaMn_{0.875}Ti_{0.125}O_3$ produced by spray pyrolysis using standardized aqueous solutions and $CaMn_{0.775}Mg_{0.1}Ti_{0.125}O_{3-\delta}$ produced from manganese oxides and titanium oxides with higher purities [11,46]. Compared to the benchmark oxygen carrier for CLC, i.e. ilmenite, which exhibits 65 % to 82 % conversion of natural gas in a similar 300 W unit [45], calcium manganite in this study achieved 90 % – 100 % of CH_4 conversion under similar operating conditions.

The attrition rate is usually used to estimate the lifetime of oxygen carriers. In general, the calcium manganite sample used in this work showed an average attrition rate in 300 W unit, i.e 0.15 wt%/h for batch 2, comparable to the best Mn ores [2]. It is comparable to that of $CaMn_{1-x-y}Mg_xTi_y$, ranging from 0.03 to 0.13 wt%/h [47]. The integrity of the material increases, e.g. by rounding of particles and the attrition rate was 0.07 wt%/h for the operations with CH_4 in the last two days, which is comparable to the best manganese ore and calcium manganite produced from high-purity raw materials.

3.5. Implications for full-scale application

The bed mass to fuel ratio of the methane tests in the batch fluidized-bed reactor is 56 kg/MW_{th}, and, for the syngas tests the mass to fuel ratio is 11 kg/MW_{th}. This is much lower than in the operational tests that were conducted in the range 150–800 kg/MW_{th} in the 300 W unit. Despite the low bed mass to fuel ratio, syngas conversion is 100 % at$\omega = 0.99$ and temperatures from 900 °C and more. For methane, conversion at $\omega = 0.99$ and 950 °C is 50 %. If this number is extrapolated to, for example, 200 kg/MW_{th}, the conversion would be above 90 %. Thus, it can be concluded that conversion is much higher in the batch reactor.

This can be explained in terms of the two-phase theory of fluidization, according to which only a minor fraction of the gas will move upwards inside the dense particle phase of a bubbling bed, whereas the majority of the gas will travel upwards in a dilute phase at high velocity, the consequence being poor contact between gas and solids. At the lower bed height of laboratory batch reactor, the two-phase flow is less developed, thus giving better contact.

However, in the full scale, assuming a fuel reactor designed similar to the riser of a circulating fluidized-bed (CFB), the conditions are much different from a bubbling bed. In such a riser, perhaps 40–50 m high, bed material would be transported upwards providing good contact between gas and solids. Examples of pressure drops measured in commercial circulating fluidized-bed boilers are 6.5–17 kPa, of which 6.5–9.6 kPa is the riser pressure drop [49]. The latter pressure drops would correspond to 65–100 kg/MW_{th} in a fuel reactor, but it could be expected that a fuel reactor would be designed and operated with higher pressure drops. Thus, the results obtained in the batch reactor with 11–56 kg/MW_{th}, clearly indicate that high gas conversion should be expected under

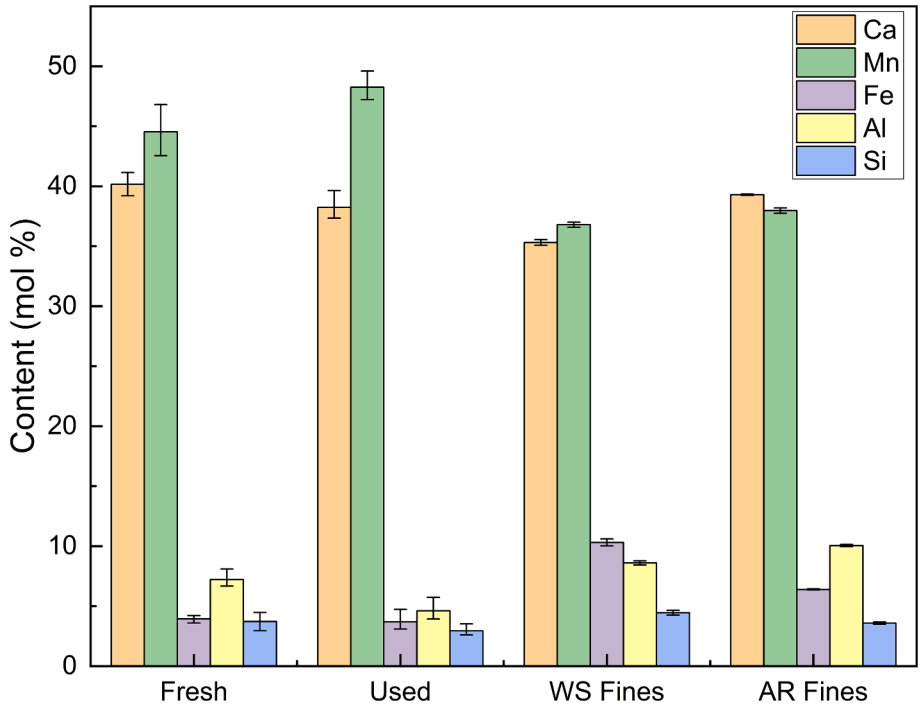

Fig. 23. Average contents of Ca, Mn, Fe, Al, Si in fresh, used calcium manganite samples and fines collected from water seal and filter for air reactor.

conditions expected for the full scale.

4. Conclusions

This study introduces the performance of calcium manganite oxygen carriers produced from a natural manganese ore and a limestone, in both batch fluidized-bed reactor and in a 300 W continuously operating CLC unit.

The calcium manganite oxygen carrier produced contained not only the expected main phase $CaMnO_3$ but also $CaMn_2O_4$. This could be attributed to the molar ratio of Ca/Mn, 0.83, as well as the presence of other components such as Fe, Al, and Si in manganese ore. Consideration should be given to using smaller raw material particle sizes and adding some excess of limestone during the manufacturing process. Notably, $CaMnO_3$ absorbs more Fe, Al, and Si present in the manganese ore compared to $CaMn_2O_4$.

The oxygen release capacity of calcium manganite increases with temperature. The oxygen release capability of fresh oxygen carriers was between 3 % and 8 % under the conditions used. Oxygen carrier calcium manganite subjected to thermal cycling exhibits relatively stable oxygen release capabilities, ranging from 2 % to 5 %.

Calcium manganite oxygen carriers give a high conversion of syngas, achieving complete conversion even at relatively low temperatures and low fuel reactor bed mass/fuel power, i.e. 850 °C and 200 kg/MW_{th}. In the case of methane, complete gas conversion is seen at high temperature and low fuel reactor bed mass/fuel power, i.e. 950 °C and above 650 kg/MW_{th}. Temperature has a significant impact on the reactivity of calcium manganite towards methane. It can be also seen that calcium manganite demonstrates relatively stable performance during prolonged high-temperature operation with methane. Batch reactor tests verified that post-operated samples showed no reduction in reactivity after 29 h of fuel operation.

Attrition was higher initially, with 1 wt%/h lost in the 2 h of syngas operation. For the last 15 h of methane operation, however, the loss was low, around 0.1 wt%/h.

CRediT authorship contribution statement

Xiaoyun Li: Writing – review & editing, Writing – original draft, Visualization, Validation, Methodology, Investigation, Formal analysis, Data curation, Conceptualization. **Robin Faust:** Writing – review & editing, Methodology, Investigation. **Victor Purnomo:** Writing – review & editing. **Daofeng Mei:** Writing – review & editing. **Carl Linderholm:** Writing – review & editing. **Anders Lyngfelt:** Writing – review & editing, Supervision, Project administration, Funding acquisition, Conceptualization. **Tobias Mattisson:** Writing – review & editing, Supervision.

Declaration of competing interest

The authors declare that they have no known competing financial interests or personal relationships that could have appeared to influence the work reported in this paper.

Data availability

Data will be made available on request.

Acknowledgments

The research has received funding from the Åforsk Foundation (Ref. 21-277).

References

[1] T. Pröll, A. Lyngfelt, Steam Methane Reforming with Chemical-Looping Combustion: Scaling of Fluidized-Bed-Heated Reformer Tubes, Energy Fuel 36 (17) (2022) 9502–9512.
[2] A. Lyngfelt, P. Moldenhauer, M. Biermann, K. Johannsen, D. Wimmer, M. Hanning, Operational experiences of chemical-looping combustion with 18 manganese ores in a 300W unit, Int. J. Greenhouse Gas Control 127 (2023) 103937.
[3] A. Lyngfelt, Chemical Looping Combustion: Status and Development Challenges, Energy Fuel 34 (8) (2020) 9077–9093.
[4] A. Lyngfelt, and B. Leckner, "A 1000 MWth boiler for chemical-looping combustion of solid fuels – Discussion of design and costs," *Applied Energy,* vol. 157, pp. 475-487, 2015/11/01/, 2015.
[5] A. Lyngfelt, D. Pallarès, C. Linderholm, F. Lind, H. Thunman, B. Leckner, Achieving adequate circulation in chemical looping combustion—design proposal for a 200 MWth chemical looping combustion circulating fluidized bed boiler, Energy Fuel 36 (17) (2022) 9588–9615.
[6] T. Mattisson, A. Lyngfelt, H. Leion, Chemical-looping with oxygen uncoupling for combustion of solid fuels, Int. J. Greenhouse Gas Control 3 (1) (2009) 11–19.
[7] A. Shulman, E. Cleverstam, T. Mattisson, A. Lyngfelt, Manganese/iron, manganese/nickel, and manganese/silicon oxides used in chemical-looping with oxygen uncoupling (CLOU) for combustion of methane, Energy Fuel 23 (10) (2009) 5269–5275.
[8] G. Azimi, H. Leion, T. Mattisson, A. Lyngfelt, Chemical-looping with oxygen uncoupling using combined Mn-Fe oxides, testing in batch fluidized bed, Energy Procedia 4 (2011) 370–377.
[9] G. Azimi, H. Leion, M. Rydén, T. Mattisson, A. Lyngfelt, Investigation of different Mn–Fe oxides as oxygen carrier for chemical-looping with oxygen uncoupling (CLOU), Energy Fuel 27 (1) (2013) 367–377.
[10] G. Azimi, M. Rydén, H. Leion, T. Mattisson, A. Lyngfelt, $(Mn_zFe_{1-z})_yO_x$ combined oxides as oxygen carrier for chemical-looping with oxygen uncoupling, AIChE J 59 (2) (2013) 582–588.
[11] M. Rydén, A. Lyngfelt, T. Mattisson, $CaMn_{0.875}Ti_{0.125}O_3$ as oxygen carrier for chemical-looping combustion with oxygen uncoupling (CLOU)—Experiments in a continuously operating fluidized-bed reactor system, Int. J. Greenhouse Gas Control 5 (2) (2011) 356–366.
[12] M. Rydén, H. Leion, T. Mattisson, A. Lyngfelt, Combined oxides as oxygen-carrier material for chemical-looping with oxygen uncoupling, Appl. Energy 113 (2014) 1924–1932.
[13] D. Jing, M. Arjmand, T. Mattisson, M. Rydén, F. Snijkers, H. Leion, A. Lyngfelt, Examination of oxygen uncoupling behaviour and reactivity towards methane for manganese silicate oxygen carriers in chemical-looping combustion, Int. J. Greenhouse Gas Control 29 (2014) 70–81.
[14] H. Leion, T. Mattisson, A. Lyngfelt, Using chemical-looping with oxygen uncoupling (CLOU) for combustion of six different solid fuels, Energy Procedia 1 (1) (2009) 447–453.
[15] P. Moldenhauer, M. Rydén, T. Mattisson, A. Lyngfelt, Chemical-looping combustion and chemical-looping with oxygen uncoupling of kerosene with Mn- and Cu-based oxygen carriers in a circulating fluidized-bed 300W laboratory reactor, Fuel Process. Technol. 104 (2012) 378–389.
[16] P. Gayán, I. Adánez-Rubio, A. Abad, L.F. de Diego, F. García-Labiano, J. Adánez, Development of Cu-based oxygen carriers for Chemical-Looping with Oxygen Uncoupling (CLOU) process, Fuel 96 (2012) 226–238.
[17] I. Adánez-Rubio, P. Gayán, A. Abad, L.F. de Diego, F. García-Labiano, J. Adánez, Evaluation of a Spray-Dried $CuO/MgAl_2O_4$ Oxygen Carrier for the Chemical Looping with Oxygen Uncoupling Process, Energy Fuel 26 (5) (2012) 3069–3081.
[18] A. Abad, I. Adánez-Rubio, P. Gayán, F. García-Labiano, L.F. de Diego, J. Adánez, Demonstration of chemical-looping with oxygen uncoupling (CLOU) process in a 1.5kWth continuously operating unit using a Cu-based oxygen-carrier, Int. J. Greenhouse Gas Control 6 (2012) 189–200.
[19] A. Lambert, C. Delquié, I. Clémeneçon, E. Comte, V. Lefebvre, J. Rousseau, B. Durand, Synthesis and characterization of bimetallic Fe/Mn oxides for chemical looping combustion, Energy Procedia 1 (1) (2009) 375–381.
[20] D. Jing, E. Hermans, H. Leion, M. Rydèn, T. Mattisson, J. Noyen, and A. Lyngfelt, *Manganese-silica combined oxides as oxygen carrier for chemical-looping combustion,* 2012.
[21] M. Arjmand, V. Frick, M. Rydén, H. Leion, T. Mattisson, A. Lyngfelt, Screening of combined Mn-Fe-Si oxygen carriers for chemical looping with oxygen uncoupling (CLOU), Energy Fuel 29 (3) (2015) 1868–1880.
[22] T. Mattisson, D. Jing, A. Lyngfelt, M. Rydén, Experimental investigation of binary and ternary combined manganese oxides for chemical-looping with oxygen uncoupling (CLOU), Fuel 164 (2016) 228–236.
[23] D. Jing, T. Mattisson, M. Ryden, P. Hallberg, A. Hedayati, J. Van Noyen, F. Snijkers, A. Lyngfelt, Innovative oxygen carrier materials for chemical-looping combustion, Energy Procedia 37 (2013) 645–653.
[24] D. Jing, T. Mattisson, H. Leion, M. Rydén, A. Lyngfelt, Examination of perovskite structure CaMnO 3-δ with MgO addition as oxygen carrier for chemical looping with oxygen uncoupling using methane and syngas, Int. J. Chem. Eng. 2013 (2013).
[25] D. Jing, F. Snijkers, P. Hallberg, H. Leion, T. Mattisson, A. Lyngfelt, Effect of Production Parameters on the Spray-Dried Calcium Manganite Oxygen Carriers for Chemical-Looping Combustion, Energy Fuel 30 (4) (2016) 3257–3268.
[26] Y. Larring, M. Pishahang, J. Tolchard, A.M. Lind, M.F. Sunding, R.E. Stensrød, M. Jacobs, F. Snijkers, T. van der Kolk, K. Albertsen, Fabrication process parameters significantly affect the perovskite oxygen carriers materials (OCM)

performance in chemical looping with oxygen uncoupling (CLOU), J. Therm. Anal. Calorim. 140 (2) (2020) 577–589.
[27] K. Mayer, S. Penthor, T. Pröll, H. Hofbauer, The different demands of oxygen carriers on the reactor system of a CLC plant – results of oxygen carrier testing in a 120kWth pilot plant, Appl. Energy 157 (2015) 323–329.
[28] A. Abad, P. Gayán, L.F. de Diego, F. García-Labiano, J. Adánez, Modelling Chemical-Looping assisted by Oxygen Uncoupling (CLaOU): Assessment of natural gas combustion with calcium manganite as oxygen carrier, Proc. Combust. Inst. 37 (4) (2019) 4361–4369.
[29] M. Källén, M. Rydén, C. Dueso, T. Mattisson, A. Lyngfelt, $CaMn_{0.9}Mg_{0.1}O_{3-\delta}$ as Oxygen Carrier in a Gas-Fired 10 kWthChemical-Looping Combustion Unit, Ind. Eng. Chem. Res. 52 (21) (2013) 6923–6932.
[30] M. Schmitz, C.J. Linderholm, Performance of calcium manganate as oxygen carrier in chemical looping combustion of biochar in a 10 kW pilot, Appl. Energy 169 (2016) 729–737.
[31] P. Hallberg, D. Jing, M. Rydén, T. Mattisson, A. Lyngfelt, Chemical Looping Combustion and Chemical Looping with Oxygen Uncoupling Experiments in a Batch Reactor Using Spray-Dried CaMn1–xMxO3– δ (M= Ti, Fe, Mg) Particles as Oxygen Carriers, Energy Fuel 27 (3) (2013) 1473–1481.
[32] A. Fossdal, E. Bakken, B.A. Øye, C. Schøning, I. Kaus, T. Mokkelbost, Y. Larring, Study of inexpensive oxygen carriers for chemical looping combustion, Int. J. Greenhouse Gas Control 5 (3) (2011) 483–488.
[33] H. Leion, Y. Larring, E. Bakken, R. Bredesen, T. Mattisson, A. Lyngfelt, Use of $CaMn_{0.875}Ti_{0.125}O_3$ as oxygen carrier in chemical-looping with oxygen uncoupling, Energy Fuel 23 (10) (2009) 5276–5283.
[34] E. Bakken, T. Norby, S. Stølen, Nonstoichiometry and reductive decomposition of $CaMnO_{3-\delta}$, Solid State Ion. 176 (1–2) (2005) 217–223.
[35] L. Liu, Z. Li, Y. Wang, Z. Li, Y. Larring, N. Cai, Industry-scale production of a perovskite oxide as oxygen carrier material in chemical looping, Chem. Eng. J. 431 (2022) 134006.
[36] M. Osman, M.N. Khan, A. Zaabout, S. Cloete, S. Amini, Review of pressurized chemical looping processes for power generation and chemical production with integrated CO_2 capture, Fuel Process. Technol. 214 (2021) 106684.
[37] A. Zaabout, S. Cloete, J.R. Tolchard, S. Amini, A pressurized Gas Switching Combustion reactor: Autothermal operation with a $CaMnO_{3-\delta}$-based oxygen carrier, Chem. Eng. Res. Des. 137 (2018) 20–32.
[38] M. Rydén, P. Moldenhauer, S. Lindqvist, T. Mattisson, A. Lyngfelt, Measuring attrition resistance of oxygen carrier particles for chemical looping combustion with a customized jet cup, Powder Technol. 256 (2014) 75–86.
[39] H. Leion, V. Frick, F. Hildor, Experimental method and setup for laboratory fluidized bed reactor testing, Energies 11 (10) (2018) 2505.
[40] S. Sundqvist, N. Khalilian, H. Leion, T. Mattisson, A. Lyngfelt, Manganese ores as oxygen carriers for chemical-looping combustion (CLC) and chemical-looping with oxygen uncoupling (CLOU), J. Environ. Chem. Eng. 5 (3) (2017) 2552–2563.
[41] C. Linderholm, A. Lyngfelt, A. Cuadrat, E. Jerndal, Chemical-looping combustion of solid fuels – Operation in a 10 kW unit with two fuels, above-bed and in-bed fuel feed and two oxygen carriers, manganese ore and ilmenite, Fuel 102 (2012) 808–822.
[42] L. Rørmark, K. Wiik, S. Stølen, T. Grande, Oxygen stoichiometry and structural properties of $La_{1-x}A_xMnO_{3\pm\delta}$ (A = Ca or Sr and $0 \leq x \leq 1$), J. Mater. Chem. 12 (4) (2002) 1058–1067.
[43] I. Staničić, J. Brorsson, A. Hellman, M. Rydén, T. Mattisson, Thermodynamic analysis on the fate of ash elements in chemical looping combustion of solid fuels – Manganese-Based oxygen carriers, Fuel 369 (2024) 131676.
[44] M. Rydén, A. Lyngfelt, T. Mattisson, Combined manganese/iron oxides as oxygen carrier for chemical looping combustion with oxygen uncoupling (CLOU) in a circulating fluidized bed reactor system, Energy Procedia 4 (2011) 341–348.
[45] M. Rydén, M. Johansson, E. Cleverstam, A. Lyngfelt, T. Mattisson, Ilmenite with addition of NiO as oxygen carrier for chemical-looping combustion, Fuel 89 (11) (2010) 3523–3533.
[46] P. Moldenhauer, P. Hallberg, M. Biermann, F. Snijkers, K. Albertsen, T. Mattisson, A. Lyngfelt, Oxygen-Carrier Development of Calcium Manganite-Based Materials with Perovskite Structure for Chemical-Looping Combustion of Methane, Energ. Technol. 8 (6) (2020) 2000069.
[47] P. Hallberg, M. Källén, D. Jing, F. Snijkers, J. van Noyen, M. Rydén, A. Lyngfelt, Experimental investigation of $CaMnO_3$ based oxygen carriers used in continuous chemical-looping combustion, Int. J. Chem. Eng. 2014 (2014).
[48] V. Thoréton, M. Pishahang, T. Mokkelbost, K. Wiik, Y. Larring, Microstructural Stability of Tailored $CaMn_{0.875-x}Fe_xTi_{0.125}O_{3-\delta}$ Perovskite Oxygen Carrier Materials for Chemical Looping Combustion, Energ. Technol. 5 (9) (2017) 1579–1587.
[49] T. Djerf, Solids Flow in Large-Scale Circulating Fluidized Bed Furnaces, Chalmers University Of Technology, Gothenburg, Sweden, 2021. PhD Thesis.